



## Review

# Sorbent-based dialysate regeneration for the wearable artificial kidney: Advancing material innovation via experimental and computational studies

Thomas Fabiani<sup>a</sup>, Maryam Zarghamidehaghani<sup>a</sup>, Cristiana Boi<sup>b</sup>, Simone Dimartino<sup>c</sup>, Sandra Kentish<sup>d</sup>, Maria Grazia De Angelis<sup>a,\*</sup>

<sup>a</sup> Institute for Materials and Processes, School of Engineering, University of Edinburgh, King's Buildings, Robert Stevenson Road, EH9 3FB, Edinburgh, Scotland, UK

<sup>b</sup> Department of Civil, Chemical, Environmental and Materials Engineering, University of Bologna, Via Terracini 28, 40131 Bologna, BO, Italy

<sup>c</sup> Institute for Bioengineering, School of Engineering, University of Edinburgh, King's Buildings, Colin Maclaurin Road, EH9 3DW, Edinburgh, Scotland, UK

<sup>d</sup> Department of Chemical Engineering, The University of Melbourne, Parkville, VIC 3010, Australia

## ARTICLE INFO

Editor: Harvey Yi Huang

## Keywords:

Hemodialysis  
Dialysate regeneration  
Adsorption  
Molecular modelling  
Wearable artificial kidney  
Uremic toxins

## ABSTRACT

Hemodialysis is the primary renal replacement therapy for patients affected by end-stage renal disease, but it has a severe impact on the patient's lifestyle and wellbeing, and is extremely water intensive. A wearable dialysis device could solve most of the issues associated with the treatment, but the main obstacle to its realisation is an efficient and reliable system for dialysate regeneration, i.e. the purification of spent dialysate from uremic toxins. Several techniques have been proposed to this aim, such as enzymatic conversion, forward osmosis and electrochemical oxidation. One of the most promising and safe technologies is adsorption, in which toxins are captured onto nanoporous materials, polymers or their combinations (mixed matrix membranes). In this review, we first give a general overview of the hemodialysis processes and of the challenges associated to making it wearable. Subsequently, we use experimental data from the literature to rank different materials based on their ability to remove the typical uremic toxins present in dialysate, including considerations on their recyclability, stability and safety. Finally, we critically analyse different computational modelling techniques available to design and/or optimise adsorbent materials for dialysate regeneration, and their accuracy in predicting the materials performance and screen large databases of adsorbents.

## 1. Introduction

## 1.1. Hemodialysis

Chronic kidney disease (CKD) is caused by the reduction of the kidneys' functionality [1–3] leading to end-stage renal disease (ESRD), that requires renal replacement therapies (RRT), such as hemodialysis (HD), peritoneal dialysis (PD) or transplantation [2]. In 2021, only 4 % of the patients starting in RRT in Europe receives a transplant: the scarcity of donors makes HD the primary treatment (81 % of ESRD patients) [4]. ESRD represents 2–3 % of the healthcare budget in developed nations, growing between 6 % and 12 % every year, despite ESRD patients represent 0.02–0.03 % of the total population. Mortality due to ESRD is 10 to 100 times greater than a control population [2] and greater than patients with cancer and heart failure (2.4 and 1.5 times, respectively) [3]. Over 2 million people worldwide rely on RRT, the majority in the US, Japan, Germany, Brazil, and Italy [2]. Furthermore,

in about 100 developing countries, representing over 50 % of the world population, only one fifth of the patients are treated. In 112 countries, with a combined population of over 600 million people, RRT is not affordable, resulting in the death of over 1 million people every year. Nonetheless, the incidence of CKD is still considered underestimated [2,3,5].

HD is an extracorporeal treatment that replaces kidney functionality, removing uremic toxins (UTs) and fluids in excess and restoring the acid-base balance. HD is based on the exchange of compounds between the blood stream and the dialysate by diffusion through a membrane, the dialyser, according to concentration gradients [6]. In HD, **vascular access** is realized through a surgical arteriovenous (AV) fistula or a central venous catheter (CVC) installed into the large veins in the neck. Vascular access often remains the most troublesome aspect of HD, since it may be prone to infections [3,7].

The **dialyser** is a membrane that retains serum proteins and blood cells [1,8] while maximizing the clearance of UTs. HD membranes are

\* Corresponding author.

E-mail address: [grazia.deangelis@ed.ac.uk](mailto:grazia.deangelis@ed.ac.uk) (M.G. De Angelis).

categorized according to their hydraulic permeability into low-flux ( $<1520 \text{ L m}^{-2} \text{ h}^{-1} \text{ MPa}^{-1}$ ) and high-flux membranes ( $>1520 \text{ L m}^{-2} \text{ h}^{-1} \text{ MPa}^{-1}$ ) [1], the latter ones being characterised by larger pore diameter (around 3 nm) and an increased nominal molecular weight cut-off. High flux dialysers allow better clearance of middle-to-large molecules and shorter treatments, but there are concerns of back diffusion of contaminants from the dialysate to the blood and inadequate solute removal [9–12].

The removal of toxins in HD is expressed in terms of clearance, defined as the volume of blood completely purified of the toxin per unit time [13]. The surface area of most dialysers ranges between 0.8 and 2.1  $\text{m}^2$  [3,14,15]. The blood stream flow in the dialyser is usually between 200 and 500  $\text{mL min}^{-1}$ : during a single session, the patient's entire blood volume flows through the dialyser every 15 min. On the other side, the dialysate is pumped up to 600–800  $\text{mL min}^{-1}$  to maximize clearance [3,14]. An adequate transmembrane pressure is maintained across the dialyser, to draw the excess liquid from the patient's blood stream. The fresh dialysate is composed of salts and glucose in ultrapure water, in a proportion to match specific concentrations of ions (Table S1) at 35–37 °C [3,16]. Every session demands ~ 120 L of dialysate [17,18]. Quality standards for the water used in dialysate are extremely strict, as the presence of low concentration of metals or bacterial contamination may lead to severe clinical consequences [19]. The ultrapure water is produced from a larger amount of tap water (280–500 L) that passes, if needed, through a softening stage, an activated charcoal filter to remove organic contaminants, and a reverse osmosis (RO) system [14,17,18]. The regeneration of spent dialysate through removal of UTs and maintenance of stable pH and electrolyte concentrations would require a much smaller volume of dialysate (from 120 L down to 0.5 L) [20].

### 1.2. Challenges of conventional hemodialysis and possible alternatives

The HD treatment is generally delivered in sessions of 4–5 h, two or three times per week, in a clinic. The intracorporeal build-up of liquid before the therapy causes vascular stress, due to the extremely reduced diuretic activity, with symptoms like muscular cramps, fatigue, and discomfort [3,21]. The duration of the sessions and the post-treatment hangover severely impact life quality [22]. An extended treatment time generally alleviates the symptoms [3], improves dialysis efficiency and solute clearance [3] but needs to be delivered close to the patient, requiring portability of the HD machine [23].

**Nocturnal and home HD** (NHD and HHD) use similar machines to in-clinic treatment: the first one is carried out 5–6 times per week, during sleep, for 6 to 8 h, while HHD is performed during the day for 2 to 4 h, with the same frequency of nocturnal HD. Both techniques mitigate the morbidity and mortality rate and improve the patients' quality of life [3,24–26]. HHD has been very differently adopted in different geographic areas: in countries like Australia and New Zealand it has been implemented safely for 50 years thanks to geographical reasons, reimbursement schemes, appropriate policies and lower cost [27]: almost 50 % of all dialysis patients in New Zealand are treated at home. Most patients in HHD have a partner or family member to assist with set-up, fluid administration, pack-up and needling, commonly on a AV-fistulae [25]. In Scotland, on the other hand, the population of patients receiving RRT at home is a minority (~11 %) and of those, only few (18.7 %) are on home hemodialysis (HHD) [28].

The benefits of more continuous forms of HD are accompanied by some drawbacks: a more frequent vascular access, that may contribute to its loss, the patients' feelings of isolation, and aggravated energy and water consumption. Lack of motivation and confidence, fear of self-cannulation and needles, inability to sleep during treatment, and a lack of family/partner are the most common barriers preventing the switch from in-centre HD to HHD [26,27]. The Australian HHD program showed that, to ensure a high qualitative standard for water, the installation of well-designed RO equipment and relative plumbing were

essential, together with a strong connection with the local authorities that control water quality [27].

HHD machines such as the NxStage and 2008 K@home™ from Fresenius [29], Quanta [30,31] and Tablo [32] are compact devices, but they are still not portable or wearable, as they must be equipped with a purification unit connected to a water supply, or use large purified water bags, with a total weight always higher than 30 kg, without the RO system. HD is still a water and energy intensive treatment (each session demands one fifth of the total energy consumed by a household per day [33]). The miniaturisation of HD would be a giant leap for millions of patients, their families and the healthcare systems. Technically, the major bottleneck for miniaturization of HD is the water feed: complete or partial regeneration of the spent dialysate would reduce the amount of water needed in each session, and lead to the desired size reduction. The regeneration unit could be adapted to current dialysers, and may be realised with a relatively wide range of materials, with less restrictions with respect to the dialyser materials that are in direct contact with the blood.

### 1.3. Classification of uremic toxins

UTs are those compounds whose accumulation in the patient is associated with the appearance of the uremic syndrome [34]. Inorganic compounds (e.g., water, sodium, phosphate, potassium) are generally excluded from this classification, despite being removal targets in dialysis [35]. A way to classify UTs is based on size, as follows:

- small, free water-soluble UTs ( $< 500 \text{ Da}$ ), such as urea, creatinine, uric acid.
- small molecular weight ( $< 500 \text{ Da}$ ), water-soluble, protein-bound uremic toxins (PBUTs), namely UTs with affinity to binding sites of proteins present in blood (e.g. human serum albumin), such as indoxyl sulfate (IS) or p-cresyl sulfate [34,36].
- middle-size ( $500 \div 12000 \text{ Da}$ ) water-soluble UTs, such  $\beta$ -microglobuline.
- high molecular weight ( $>12000 \text{ Da}$ ), such as lipoproteins [37,38].

Small water-soluble UTs are easy to dialyse, due to their fast diffusivity, and their clearance is generally flow-limited. Middle-size water-soluble UTs clearance is membrane-limited, while PBUTs clearance with conventional HD is challenging due to their extremely low concentration in the free state [34,36]. Presence of UTs in the dialysate depends on the quantities dialysed, influenced by their concentrations in the blood stream and their permeabilities through the dialyser. However, due to the large volume of water used in conventional HD, UTs concentrations in dialysate are extremely low. The transport across the HD membrane is bidirectional and non-specific so that all substances can move in either direction, according to their concentration gradient [39]. As a consequence, non-toxic components, like glucose and amino acids, are cleared as well and toxic compounds like endotoxins or metals, can enter the bloodstream from the dialysis fluid compartment [39] which may trigger biological reactions of different severity. Although such aspects are beyond the scope of the present paper, it is important to point out that the presence of other components in spent dialysate such as mono and divalent ions as well as glucose, L-lactate, glycerol and a set of amino acids (namely proline, valine, glycine, glutamate, alanine, and leucine) [40] may affect the adsorption process [41], and these effects have been addressed in some of the papers reviewed here.

The typical UTs in spent dialysate are urea [42], creatinine, uric acids,  $\alpha$ 1-acid glycoprotein, phenylacetic acid, phenylacetylglutamine, retinol binding protein (RBP), creatine, and hippuric acid [43]. Shao *et al.* reported the 30 most abundant UTs removed during a thrice-weekly dialysis session, using a high-flux dialyser [40,43] (see Table 1 and Fig. 1) their reference concentrations are used in this work to compare experimental data available in the literature.

Urea is the universal marker of UTs clearance, dialysis adequacy and

**Table 1**

Uremic toxins (small-sized) and relative reference concentrations and per-session dialysed amount used in this review for comparison of experimental data. [53].

Uremic toxin	Reference concentration μM	Amount dialysed per-session mg
Urea	5000.0	23600.0
Creatinine	74.3	1650.0
Uric acid	244.0	1000.0
Hippuric acid (HA)	8.4	464.0
Indoxyl sulphate (IS)	2.8	86.4
3-indoloacetic acid (IA)	1.7	17.1

therapy dosing, due to its high concentration and ease of measurement [36], although many UTs have a different kinetic behaviour [44]. The daily production of urea is between 240 and 470 mmol (14–28 g) [45] and its concentration ranges from 1.8 to 7.1 mM in a healthy patient [46], to about 4–5 times this value in patients in HD [43,47]. In the spent dialysate, urea concentration may be as high as 11 mM at the beginning of a conventional HD session and decreases exponentially [42]. Urea is generally considered to have negligible toxicity, although recent studies have shown that its accumulation can favour several adverse health effects [35,36,48–52].

Metabolomics and proteomics have revealed several new compounds accumulating in CKD patients' blood, ranging from small molecules to peptides and small proteins [34,36,38,54–56]. The EuTox open database [43] collected 67 water-soluble UTs, 30 middle-size UTs and 33 PBUTs associated with CKD. Other classifications rely on chemical similarities, metabolic pathways, or toxicity [56–58]. There is no consensus on the role of any single toxin to the clinical outcomes observed in CKD patients [35]. Vanholder *et al.* [35,44,58–60] ranked UTs according to their toxicity, considering proven *in vivo*, *ex vivo*, or *in vitro* effects on biological systems, setting p-cresyl sulphate first and in decreasing order, beta-microglobulin, asymmetric dimethyl arginine (ADMA), kynorenes, carbamylated compounds, fibroblast growth factor-23 (FGF-23), interleukin-6, tumor necrosis factor- $\alpha$  (TNF- $\alpha$ ) and symmetric dimethyl arginine (SDMA) [58].

In our opinion, the current classification of UTs, solely based on physiochemical properties and ease of clearance, should also incorporate clinically-oriented parameters, such as the degree of toxicity, in an effort to achieve a dialysis treatment with better clinical outcomes. To this aim, the adoption of a multidisciplinary approach, including clinical and engineering expertise, is crucial to innovate HD technology and improve outcomes for patients.

## 2. Technologies for uremic toxins removal from spent dialysate

### 2.1. Enzymatic conversion, forward osmosis and oxidation

In previous attempts to make the HD machine portable and/or wearable, the regeneration of spent dialysate was mostly carried out via a multi-cartridge system [61]: toxins with low polarity or poor water solubility were adsorbed on hydrophobic supports and ionic concentration was effectively rebalanced with ion exchange resins [62,63]. The complete removal of urea was achieved enzymatically, as described in more detail in the following paragraph. A more recent approach is the bioartificial kidney, based on renal proximal tubule cells cultured on artificial membranes, as described by Ramada *et al.* [63]. The removal of urea and other UTs in HD-related processes has been reviewed in previous works: Shao *et al.* analysed competition effects, with a focus on photoelectrochemical strategies [64]; Ma *et al.* focused on adsorption-based strategies for removing UTs from blood [65], while enzymatic, electrochemical and physiochemical methods for urea removal were reviewed by van Gelder *et al.* [20]. Strategies for PBUTs removal are addressed in several review papers, describing adsorption,

displacement, and other techniques [66–69]. In this review, the emphasis is placed on technologies and materials suitable for the adsorptive removal of UTs from dialysate, along with the efforts dedicated to model at molecular level the materials for such application. A brief overview of other methods evaluated for UTs removal from dialysate, namely enzymatic conversion, forward osmosis and photoelectrocatalytic oxidation is provided below.

The **enzymatic conversion of urea** relies on urease, an enzyme that oxidizes the molecule into ammonium and carbon dioxide, with high selectivity. The Recirculating Dialysis (REDY) Sorbent System was the first device for portable HD performing dialysate regeneration through a multi-cartridge technology, with a total weight of 5 kg (including dialysate) [17]. In the REDY system, an activated carbon layer removed heavy metals, oxidants, chloramines, and other organic molecules. Urea was enzymatically converted to ammonium and carbonate ions. Ammonium is highly toxic and was captured by a third layer, a cation exchanger (zirconium phosphate), which also eliminated calcium, magnesium, potassium, releasing sodium and protons into the dialysate. A final layer of zirconium oxide and zirconium carbonate adsorbed anions such as phosphates, fluoride, and heavy metals, while exchanging bicarbonate and small amounts of acetate. The dialysate leaving the cartridge was a near-ultrapure solution [61,70,71]. The device, commercialised between 1973 and 1993, was withdrawn from the market because of aluminium leachate, suspected of causing fracturing osteomalacia and encephalopathy, probably coming from the Al<sub>2</sub>O<sub>3</sub> support on which the enzyme was immobilized [20]. Other technologies with the same design concept have been recently developed with a focus on miniaturization and weight reduction, better control of the dialysate composition, alternative supports for enzyme immobilization, and different materials for ion-exchange. These devices have a weight ranging between 10 and 30 kg (including dialysate) [17]. The prototype from Gura *et al.* named WAK (Wearable Artificial Kidney), has been the only one, to our knowledge, to have reached a FDA-approved human trial. The trial was discontinued as it encountered issues with flow control and CO<sub>2</sub> bubble formation due to the chemical decomposition of urea by urease [62]. Other prototypes were developed by NeoKidney (Dutch Kidney Foundation and Debiotech SA), AWAK Pty Ltd, Dharma™ EasyDial and Next kidney [72]. Next Kidney adsorbent and devices from Medtronic and Fresenius are similar to REDY with different supports for urease/design/layers. Van Gelder *et al.* provided an overview of portable devices for HD and PD [17].

**Forward osmosis (FO)** is a process based on a semi-permeable membrane, through which water permeates, driven by a difference in osmotic pressure. A solution with high osmotic pressure, known as a draw solution, is used to recover water from the feed stream [73]. Commercially available dialysate concentrates, with high osmotic pressure, can be used as draw solutions, to recover clean water from the spent dialysate, at the same time being diluted to the desired concentration. Fig. 2 demonstrates the mechanism of water recovery through the FO process [74]. While FO membranes exhibit high rejection towards compounds such as ions, glucose, charged molecules or other UTs, urea rejection remains relatively low and drops with increasing urea concentration [73]. Commercial membranes composed of cellulose triacetate, exhibited an average rejection of urea (at 32 mM) equal to 78 %, however concentrating the spent dialysate between 1.8 and 2.8 times, rejection dropped to 34.6 %. Creatinine and uric acid were not detected in the draw solution. [75–77]. Hollow-fibre Aquaporin membranes, namely biomimetic membranes containing aquaporin channel proteins, are currently marketed to reduce the water consumption in HD by two thirds, but there are no data available for urea rejection [78]. Consequently, FO has seen minimal application for the separation of urea solutions [79,80], and at present it may be difficult to implement in a wearable device. However, FO shows potential in the improvement or replacement of RO systems. [76–78].

**Photoelectrocatalytic oxidation** employs a light source and a catalytic support, such as TiO<sub>2</sub> electrodes, to oxidize urea in spent dialysate

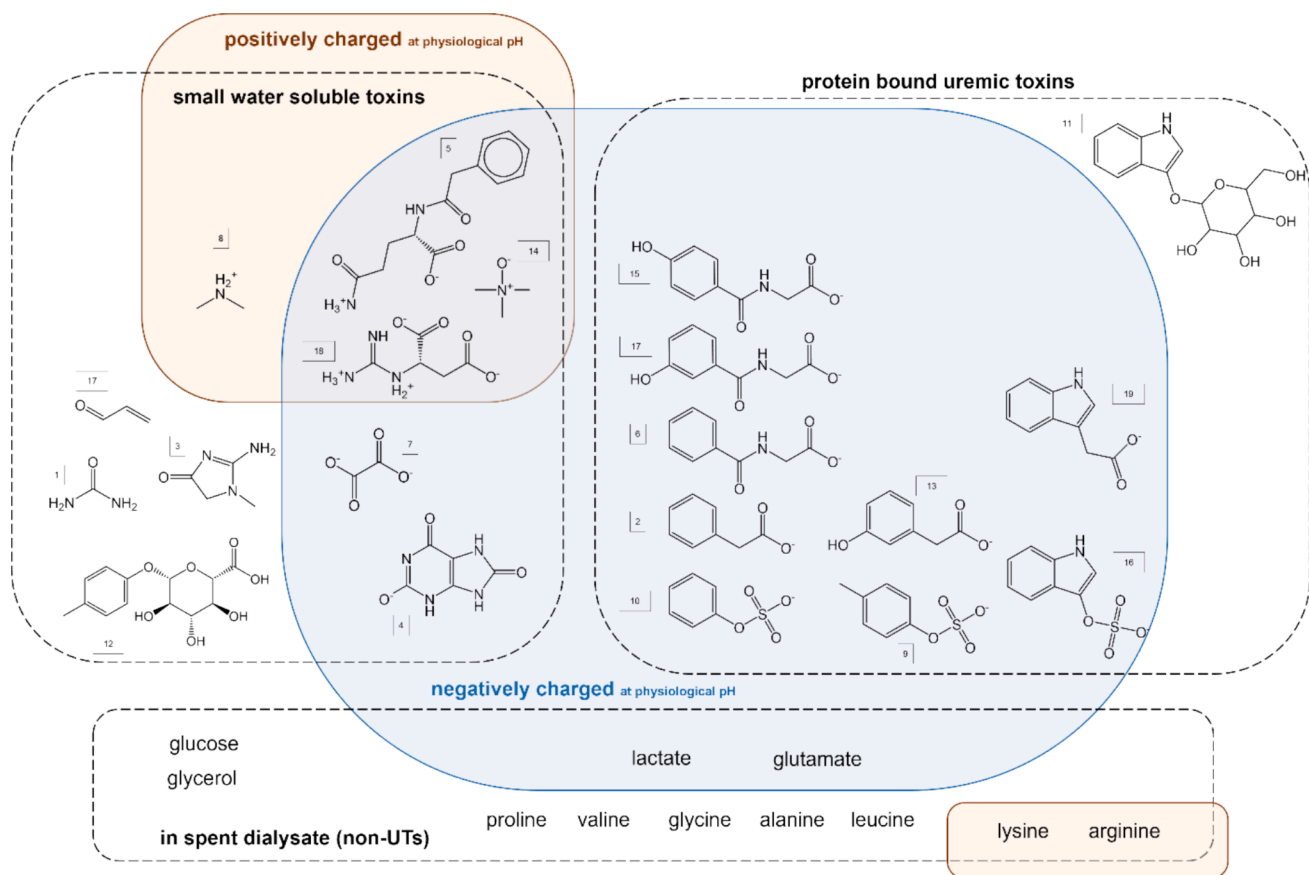


**Fig. 1.** Most abundant compounds in the spent dialysate: small water-soluble compounds, PBUTs and other compounds (non UTs). Middle sized toxins are omitted. Chemical structures display the charges relative to their dissociation at physiological pH (7.8). UTs are reported according to their amount dialysed in a session, according to Shao et al. [40]. (1) urea (2) phenylacetic acid (3) creatinine (4) uric acid (5) phenylacetylglutamine (6) hippuric acid (7) oxalate (8) dimethylamine (9) p-cresyl sulphate (10) phenyl sulphate (11) indoxan (12) p-cresyl glucuronide (13) 3-hydroxyphenylacetic acid (14) trimethylamine-n-oxide (15) 4-hydroxyhippuric acid (16) indoxyl sulfate (17) acrolein (18) guanidinosuccinic acid (19) indole-3-acetic acid.

into  $N_2$  and  $CO_2$ . This approach offers the advantages of low power consumption and a compact electrode, with an area between 0.18 and 0.5  $m^2$ , sufficient to remove the daily urea production [40,53,81,82]. Nonetheless, the selectivity of oxidation as well as the formation of by-products and other active species are still an open issue. The use of an activated carbon treatment could reduce the amount of side products, removing the cytotoxic effect of the spent dialysate after the photo-electrocatalytic treatment [40]. On the other side a FO system may protect the electrode from reducing compounds in the dialysate (e.g. glucose) and prevent the back diffusion of side products of the oxidation [53]. A comprehensive review of electro-chemical technologies for urea

oxidation was presented by Van Gelder *et al.* [20].

## 2.2. Adsorption-based technologies

Adsorption involves the uptake of molecules from a fluid phase onto a solid in contact with it, and is governed by different types of interactions e.g. dispersion forces, hydrogen bonding, electrostatic interactions, polarization, and covalent bonding [83]. The static binding capacity,  $q_{eq}$  ( $mg\ g^{-1}$ ), is the amount of adsorbate captured per unit mass of solid adsorbent in equilibrium with a concentration  $c_{eq}$  (mM) of adsorbate in the fluid phase. The static **binding capacity**  $q_{eq}$  in

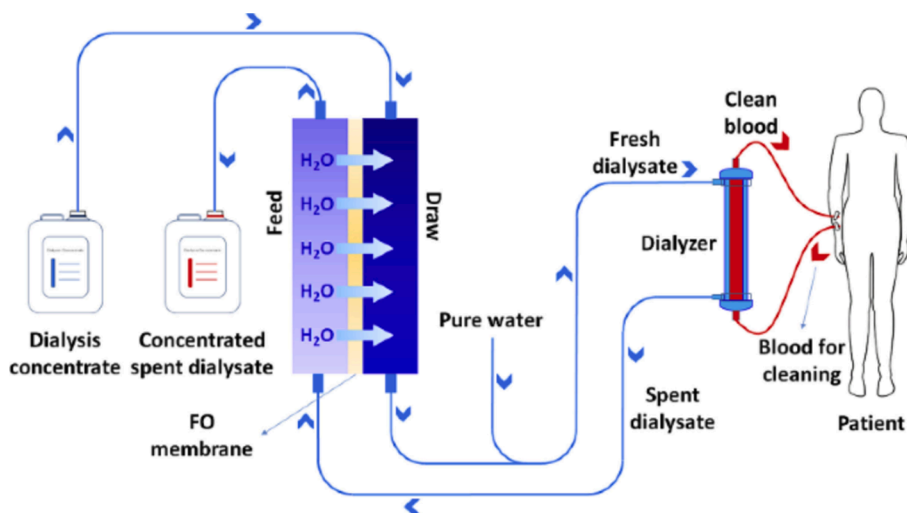


Fig. 2. Schematic an FO process to recover water from spent dialysate stream [75].

equilibrium with a UT target concentration  $c_{eq}$  corresponding to the desired value in the dialysate at the end of the session was employed as metric to compare materials. In the case of urea, the target concentration in the liquid phase was 5 mM, while values for the other toxins are reported in Table 1, together with the amount that needs to be removed per session.

Nanoporous materials, characterized by high specific surface area, are often employed as adsorbents due to the high number of adsorption sites, according to dimensions and configurations of the pores and surface functionalization [84]. Nanoporous materials may be used as fillers, dispersed in a polymeric matrix, to form composites, named mixed matrix membranes (MMM). MMMs couple the adsorbing properties of the nanoporous materials with the optimal fluid dynamic and transport properties of the porous polymeric matrix. Polymers themselves can swell, be highly porous and used as adsorbents; furthermore, they may be easily functionalized and manufactured [85]. In the next sections, the current development and testing of adsorbents for urea adsorption are reviewed.

### 2.2.1. Nanoporous materials and mixed matrix membranes

**Activated carbon (AC)** is a porous amorphous material obtained by the physical or chemical activation of a carbonaceous source to increase the specific surface area for adsorption [86,87]. AC has been widely used for water purification from heavy metals and pollutants, is inexpensive and widely available. On the other hand, AC is not selective for urea and has a low binding capacity ( $8.8 \text{ mg g}^{-1}$  at 10 mM [88],  $6 - 14.4 \text{ mg g}^{-1}$  at 20 mM [20]), requiring 2–5 kg for the removal of daily produced urea [17,89]. For this reason, AC is frequently incorporated into the design of regenerating systems to capture other UTs. For instance, a hundred grams of AC would adsorb the amount of creatinine dialysed in a session,

keeping the concentration in the dialysate lower than  $88.4 \text{ }\mu\text{M}$  [40,88] (considering a  $q_{eq}$  of  $17.4 \text{ mg g}^{-1}$  [88]). Furthermore, a mixed matrix membrane (MMM) dialyzer including AC particles was fabricated to enhance the clearance of PBUTs (hippuric acid, indoxyl sulfate and creatinine) and prevent endotoxin contamination [90,91].

Other commercial adsorbents commonly used for water treatment are **zeolites**, aluminosilicates with a microporous crystalline structure. Zeolites may contain aluminium atoms in their structures (with the potentially toxic effects discussed above) forming acid sites with a negative charge, counterbalanced by the presence of a cation. Zeolites were investigated for UTs sorption [92], and successfully incorporated in a polymeric matrix to form a MMM with the same scope [93–95] (Table 2). The chemical structures of four types of zeolites tested for UTs (MOR, MFI, and STI, FAU) are shown in Figure S1. Despite their good selectivity, they suffer from a low binding capacity for urea [20]. For example, a ZSM-5 zeolite (MFI, with an initial Si/Al ratio of 400), was shown to adsorb  $6.36 \text{ mg}$  of urea per gram of zeolite at 20 mM of urea in the solution after undergoing de-alumination [96]. Cheng *et al.* reported ZSM-5 to adsorb  $6.63 \text{ mg g}^{-1}$  of urea at 4.5 mM [89]. Wernert *et al.* tested several zeolites for urea adsorption in water, reporting silicalite (MFI, Si/Al  $\rightarrow \infty$ ) to adsorb  $28.97 \text{ mg g}^{-1}$  in a solution of 7.4 mM. At a similar concentration, mordenite (MOR, Si/Al equal to 10) adsorbed  $2.49 \text{ mg g}^{-1}$  of urea at 8.5 mM [92], almost one order of magnitude lower. Conversely, MOR type (with Si/Al ratio equal to 10, zeolite CBV 20A) showed the best performance for creatinine, with an adsorption of  $4.77 \text{ mg g}^{-1}$  at  $49.8 \text{ }\mu\text{M}$  (creatinine concentration in a healthy patient is  $74.35 \text{ }\mu\text{M}$ ), outperforming all the other zeolites tested [53]. MFI (silicalite) adsorbed  $1.07 \text{ mg g}^{-1}$  at  $91.8 \text{ }\mu\text{M}$  of creatinine [92].

Stilbite may adsorb  $1.2 \text{ mg}$  of uric acid per gram of solid adsorbent with  $c_{eq}$  of  $95.3 \text{ }\mu\text{M}$  (uric acid concentration in a healthy patient is

Table 2  
Zeolites as adsorbents for UTs.

Zeolite	Type	Al/Si	UT	Buffer	Binding capacity $q_{eq}$ ( $c_{eq}$ ) $\text{mg g}^{-1}$		Ref.
ZSM-5	MFI	400 *	urea	Phosphate Buffer Solution (PBS)	6.4	(20 mM)	[96]
ZSM-5	MFI	400	urea	PBS	6.6	(4.5 mM)	[89]
silicalite	MFI	$\infty$	urea	Deionized (DI) water	28.9	(7.4 mM)	[92]
silicalite	MFI	$\infty$	creatinine	DI water	1.1	(91.8 $\mu\text{M}$ )	[92]
mordenite	MOR	10	urea	DI water	2.5	(8.5 mM)	[92]
mordenite	MOR	10	creatinine	DI water	4.8	(49.8 $\mu\text{M}$ )	[92]
stilbite	STI **	2.8	uric acid	DI water	1.2	(95.3 $\mu\text{M}$ )	[92]
690-HOA	MOR	240	creatinine	DI water	0.4	(131 $\mu\text{M}$ )	[99]

\* after dealumination,

\*\* Cation ratio  $\text{Ca}^{2+}$  9.0 % and  $\text{Na}^{+}$  2.3 %.

244–304  $\mu\text{M}$  [53]), therefore more than 1 kg of this zeolite would be needed to capture the uric acid dialysed in a session [92]. Moreover, the same zeolite seemed to have a fair selectivity (with respect to other materials) to capture indoxyl sulphate, with a binding capacity of 0.136  $\text{mg g}^{-1}$  at 17 mM (despite the target concentration is 2.8 mM).

Zeolites were also introduced into membranes to form MMMs to adsorb urea, creatinine, and uric acid. These were fabricated through non-solvent induced phase inversion (NIPS), dispersing de-aluminated HEU clinoptilolite ( $\text{Si/Al} = 4$ ), ZSM-5 and AC into in an asymmetric porous membrane of cellulose acetate. According to this study, 75 g of HEU clinoptilolite were sufficient to adsorb the daily production of creatinine; while for uric acid, AC still appears to be the best adsorbent. The MMM was able to retain the water permeability of the pristine membrane and showed minor aggregation of the filler [96,97].

Ebara *et al.* directed their attention towards incorporating zeolites into an electrospun polymer matrix. A nanofiber made of poly(ethylene-co-vinyl alcohol) (EVOH), with an ethylene content of 44 % mol, in which zeolites were dispersed up to 10 % wt, was tested as a creatinine adsorbent [93]. Adsorption efficiency decreased by increasing the zeolite concentration due to the aggregation of the zeolites. The authors claimed that 170 g of composite was necessary to remove the daily production of creatinine, roughly 1.7 times the amount of AC required to have the same binding capacity [93]. A similar protocol was used to produce composite nanofibers based on EVOH / 940-HOA (up to 44 % wt). The polymer matrix considerably reduced the cytotoxicity of the zeolite powder, but it hindered the adsorption of creatinine. The amount of adsorbed creatinine decreased with the increase in ethylene content associated with a higher crystallinity of nanofibers [98]. In another study, MOR zeolite with high silica content (690-HOA,  $\text{Si/Al} = 240$ ) was incorporated into similar nanofibers for the adsorption of indoxyl sulphate. The nanofiber mesh exhibited an adsorption capacity of 0.11  $\text{mg g}^{-1}$ , while the adsorption capacity of zeolite increased from 0.21  $\text{mg g}^{-1}$ , measured as a static adsorption test on the powder, to 0.39  $\text{mg g}^{-1}$  when it was dispersed in the nanofiber. Not least, cell viability increased from 86 % to 96 %. [99].

To conclude, zeolites and AC are cheap (1–100 USD  $\text{kg}^{-1}$  [100]) and available materials that can be embodied successfully in polymers to improve biocompatibility and fluid dynamic properties. However, aluminium in zeolites may leach from their structure, therefore a de-alumination step is necessary to ensure higher safety [101].

**Mesoporous silica** is based on silicon and oxygen atoms, but with porosity ranging between 2 – 50 nm. It may be synthesized through a sol-gel technique by the use of a precursor named (3-aminopropyl) triethoxysilane (APTES) and a surfactant, and sequentially functionalized to change surface properties [102]. Mesoporous silica with a hexagonal array of pores, known as SBA-15, was investigated for the adsorption of urea, creatinine, and hippuric acid. Pristine SBA-15 had a BET surface area of 633.0  $\text{cm}^2 \text{g}^{-1}$  and total pore volume of 1.02  $\text{cm}^3 \text{g}^{-1}$

that decreased gradually with increasing concentration of APTES used to functionalize the material. APTES increased the hydrophilicity and improved the adsorption of urea (increased from 42.3  $\text{mg g}^{-1}$  at 5 mM of urea to 64.41  $\text{mg g}^{-1}$ ) and creatinine (although the creatinine concentration was higher than that in a healthy patient), while disfavoring the adsorption of hippuric acid. [102,103]. However, SBA-15 dissolves in neutral or basic solutions, representing an issue for this application [104]. Almost 336 g of SBA-15 would adsorb urea dialysed in a session (at 5 mM). Amine functionalized mesoporous silica, synthesized through a surfactant template, has a price assessed around 600 USD  $\text{kg}^{-1}$  [100,105].

A novel class of materials are **metal organic frameworks** (MOFs), composed of metal atoms coordinating organic binders, forming two-dimensional (2D) or three-dimensional (3D) porous structures. They offer tuneable porosity and large surface areas (up to 10,000  $\text{m}^2 \text{g}^{-1}$ ) [106] and they have been extensively tested for adsorption of gases and liquids [107], as well as for adsorption of UTs (Table 3). In this section, HKUST-1, MIL-100(Fe) and UiO-66 are presented describing functionalization and fabrication strategies.

HKUST-1 (also known as Cu-BTC), based on a copper centre binding benzene-1,3,5-tricarboxylate (BTC) linkers (Figure S2a-c), was utilized to encapsulate 250  $\text{mg g}^{-1}$  of urea (from a 79 mM urea in 21 % ethanol-water solution) [108]. A new dialyzer based on a double layer material was developed using a polydopamine/polyacrylonitrile (PD/PAN) nanofiber. The fibres were used as a support for HKUST-1 growth and then covered with a chitosan-sericin nanofiber layer to ensure biocompatibility and reduce platelet and protein adhesion. The material, containing 60.2 % wt of HKUST-1, was able to adsorb 128  $\text{mg g}^{-1}$  at 2 mM of urea and 22.15  $\text{mg g}^{-1}$  creatinine (at 290  $\mu\text{M}$ , ~ 4 times the target concentration for creatinine) in deionized water. Urea appeared to preferentially bind to the HKUST-1, while creatinine seemed to interact with the chitosan/sericin fibre, as confirmed by DFT simulations (see Section 2.3) [109].

MIL-100(Fe) is a MOF based on the same BTC linker, coordinating iron atoms. It adsorbed 13.14  $\text{mg g}^{-1}$  of creatinine in equilibrium with a PBS solution (pH 7.4) of 80  $\mu\text{M}$  creatinine; such adsorption performances are comparable to those of AC [110].

UiO-66 is a MOF composed of  $[\text{Zr}_6\text{O}_4(\text{OH})_4]$  clusters with 1,4-benzodiphenylacetic acid as a ligand; different functionalization of the linker, with amine, carboxylate, sulphate groups as substituents (UiO-66-NH<sub>2</sub>, UiO-66-(COOH)<sub>2</sub>, UiO-66-SO<sub>3</sub>H), may provide additional interaction sites in the materials (Figure S2b-d). A composite material, fabricated by in-situ growth of 15.3 % wt of UiO-66-(COOH)<sub>2</sub> in a cotton fibre, showed a remarkable adsorption of creatinine of 165  $\text{mg g}^{-1}$  at 80  $\mu\text{M}$  (~10 times the creatinine adsorbed by AC) [111]. The adsorption of HA and IA was studied in UiO-66-NH<sub>2</sub>, a set of UiO-66 MOFs with different degrees of substitution with an amino group. UiO-66-NH<sub>2</sub> with 25 and 75 %mol of amino groups adsorbed 23.1  $\text{mg g}^{-1}$  of HA (at 16.83  $\mu\text{M}$ ,

**Table 3**  
MOFs (or MMM based on MOFs) as adsorbents for UTs.

MOF	Matrix	UTs	Buffer	Binding capacity $q_{\text{eq}} (\text{C}_{\text{eq}})$ $\text{mg g}^{-1}$		Ref.
HKUST-1	PD/PAN	Urea	DI water	128 213	(2 mM) in the composite (2 mM) in the filler	[109]
MIL-100(Fe)	not in MMM	Creatinine	PBS 1 mM, pH 7.4	13	(80 $\mu\text{M}$ ) in the filler	[110]
UiO-66-(COOH) <sub>2</sub>	cotton	Creatinine	Tyrode buffer	165 1100	(80 $\mu\text{M}$ ) in the composite (80 $\mu\text{M}$ ) in the filler	[111]
UiO-66-(COOH) <sub>2</sub>	PLA	IS HA	Tyrode buffer	1.2 < 1.0	(HA, 17 $\mu\text{M}$ ) in the composite (IS, 2.8 $\mu\text{M}$ ) in the composite	[114]
UiO-66-SO <sub>3</sub> H	PLA	IS HA	Tyrode buffer	1.2 < 1.0	(HA, 17 $\mu\text{M}$ ) in the composite (IS, 2.8 $\mu\text{M}$ ) in the composite	[114]
UiO-66	PLA	IS HA	Tyrode buffer	1.2 < 1.0	(HA, 17 $\mu\text{M}$ ) in the composite (IS, 2.8 $\mu\text{M}$ ) in the composite	[114]
UiO-66-NH <sub>2</sub> 25 and 75 mol %	not in MMM	HA 3-indoloacetic acid	DI water / protein	23.1 27.1	(17 $\mu\text{M}$ ) in the filler (0.06 $\mu\text{M}$ ) in the filler (75%)	[112]

with a target concentration of 8.4  $\mu\text{M}$ ), and 27.1  $\text{mg g}^{-1}$  of IA (0.06  $\mu\text{M}$ , almost 28 times lower than the target concentration), at 20 °C [112].

UiO-66, UiO-66-SO<sub>3</sub>H, and UiO-66-(COOH)<sub>2</sub> incorporated into a poly-lactic acid (PLA) matrix were tested for adsorption of HA and IS. UiO-66-SO<sub>3</sub>H with a binding capacity of 46.7  $\text{mg g}^{-1}$  (+55 % with respect of the pristine UiO-66) outperformed the other two UiO-66 MOFs, in a Tyrode's buffer solution, similar to PBS, but also containing bicarbonate and glucose [113]. However, the variation of binding capacity, at relevant concentrations of these toxins (2.8  $\mu\text{M}$  for IS and 8.73  $\mu\text{M}$  for HA), was relatively modest [114].

The poor stability of MOFs in the presence of water vapor and liquid water is a well-documented issue, posing concerns about their use in HD applications. For instance, HKUST-1 showed structural damage and crystallinity loss when placed in deionized water [115]. Even ZIF-8 and UiO-66, known for their stability against moisture in gas adsorption applications, were shown to be poorly stable in a buffer solution containing multivalent ions, such as the spent dialysate [116]. Hydrolysis may be seen as substitution reaction, in which water molecules (or hydroxide ions) replace metal coordination linkers. Such reaction depends on the alkalinity of organic ligands, the strength of metal coordination bonds, and the functional groups shielding the coordination sites. Strong coordination bonds or significant steric hindrance promote MOFs stability, preventing the attack of guest molecules or the intrusion of the guest into metal nodes [117]. The combination with a polymer matrix in a MMM or a superficial coating may preserve the structure of the MOFs [118].

HKUST-1, similarly to other MOFs, have a selling price of 7380 USD  $\text{kg}^{-1}$ , that in case of mass-scale production (via mechanochemical liquid-assisted grinding and aqueous synthesis) was assessed to decrease between 2 and 3 order of magnitude, becoming competitive with other conventional adsorbents [105].

Inorganic nanomaterials such as MXenes and molybdenum disulfide (MoS<sub>2</sub>) were also considered for UT adsorption from spent dialysate. Their adsorption capacities under static ( $q_{eq}$ ) and dynamic ( $Q_e$ ) conditions are reported in Table 4. MXenes are 2D materials with the general structure of  $\text{M}_{n+1}\text{X}_n\text{T}_x$ , in which M represents an early transition metal (such as Ti, V, Nb, Mo), X is C and/or N, while  $\text{T}_x$  represents surface terminations, and n ranges between 1 and 4. In  $\text{Ti}_3\text{C}_2\text{T}_x$ , three layers of Ti atoms are interleaved with two layers of carbon atoms, with surface terminations such as -OH, -O-, and -F bonded to the outer Ti layers. Water and organic molecules, such as hydrazine, urea, and cationic dyes can be intercalated reversibly into the MXene layered structure.  $\text{Ti}_3\text{C}_2\text{T}_x$  proved to have a fairly low adsorption of urea, equal to 13.8  $\text{mg g}^{-1}$  at 20 mM in aqueous solution at 37 °C. Despite the low uptake, adsorption from dialysate is 99 % of that from the aqueous solution, suggesting the high selectivity of MXene  $\text{Ti}_3\text{C}_2\text{T}_x$  for urea due to the narrow slit pores

[119].  $\text{Ti}_3\text{C}_2\text{T}_x$  adsorbed 17.3  $\text{mg g}^{-1}$  of creatinine from aqueous solution, at concentrations of 115  $\mu\text{M}$ , similarly to AC [120].  $\text{Ti}_3\text{C}_2\text{T}_x$  proved to neither induce early apoptosis nor platelet activation, without disrupting cell viability, confirming its great potential for blood contact applications [121].

**Molybdenum disulfide (MoS<sub>2</sub>)** is a layered dichalcogenide of transition metals with hexagonally packed structures in which Mo layers are located between two closely arranged S layers (Figure S3) [122]. The structure possesses adjustable layer spacing and the presence of defects showed to promote urea adsorption, up to 63.9  $\text{mg g}^{-1}$  at 2.3 mM in MoS<sub>2</sub> with widened interlayer spacing (WDR-MoS<sub>2</sub>) [123]. MoS<sub>2</sub> nanosheets decorated with cerium oxide CeO<sub>2</sub> (MoS<sub>2</sub>-CeO<sub>2</sub>) showed a static binding capacity of 83.66  $\text{mg g}^{-1}$  and 90.6  $\text{mg g}^{-1}$  at 2.1 and 3.5 mM of urea respectively, in water solution. At this concentration the adsorption isotherm is not linear, suggesting that the material, in that range of concentration, is approaching the maximum adsorption capacity. MoS<sub>2</sub>-CeO<sub>2</sub> may adsorb 68.8  $\text{mg g}^{-1}$  of creatinine at 126  $\mu\text{M}$  and 49.5  $\text{mg g}^{-1}$  of uric acid at 164  $\mu\text{M}$ , demonstrating acceptable performance properties, exceeding AC sorption (Table 4). Almost 260 g of MoS<sub>2</sub>-CeO<sub>2</sub> adsorbent would adsorb urea dialysed in each session, keeping the concentration of 3.5 mM of urea in the dialysate. In addition, MoS<sub>2</sub>/CeO<sub>2</sub> have good hemocompatibility and cell compatibility [124].

MoS<sub>2</sub>-based materials showed an important decrease in UTs adsorption capacity in aqueous solution in dynamic tests [123,124] (Table 4). Dynamic testing involves flowing a constant concentration of a single toxin through a material packed in a column, ensuring a continuous flow, resembling the conditions in a regeneration unit. For this experiment, materials were tested using solutions of 2.6 mM of urea, 884 mM of creatinine (10 times the target concentration), or 356 mM of uric acid. WDR-MoS<sub>2</sub> adsorbed 38.4, 53.1 and 23.1  $\text{mg g}^{-1}$ , while MoS<sub>2</sub>-CeO<sub>2</sub> adsorbed 59.1, 53.7, and 25.1  $\text{mg g}^{-1}$  of urea, creatinine, and uric acid respectively. The observed decrease in adsorption may be ascribable to diffusional limitations within the packed column and they may be mitigated by dispersing the adsorbent powder within a polymer matrix, as demonstrated with zeolites [96,99]. A further decrease of the dynamic adsorption capacity for urea (-48 % and -51 %), creatinine (-38 % and 52 %), and uric acid (-40 % and 56 %) was observed, when employing a mock dialysate solution, revealing the negative impact of ionic strength on UTs adsorption in WDR-MoS<sub>2</sub> and MoS<sub>2</sub>-CeO<sub>2</sub>. Such behaviour is probably related to the interference of cations in the solution [123]. A similar mechanism is proposed for MoS<sub>2</sub>/CeO<sub>2</sub> [124]. To the best of our knowledge, WDR-MoS<sub>2</sub> and MoS<sub>2</sub>-CeO<sub>2</sub> are not produced on a commercial scale; on the other hand MoS<sub>2</sub>, prepared via a solvothermal method, has a selling price assessed between 520 and 2945 USD  $\text{kg}^{-1}$  [125].

**Table 4**  
Inorganic nanosheets for UT sorption: MXene and MoS<sub>2</sub>.

Material	UTs	Aqueous static binding capacity		Aqueous dynamic binding capacity		Dialysate dynamic binding capacity		Ref.
		$q_{eq}(c_{eq})$ $\text{mg g}^{-1}$	(concentration)	$Q_e(c_{eq})$ $\text{mg g}^{-1}$	( $c_{eq}$ )	$Q_e(c_{eq})$ $\text{mg g}^{-1}$	( $c_{eq}$ )	
$\text{Ti}_3\text{C}_2\text{T}_x$ MXene	urea	13.8	(20 mM)					[119]
	creatinine	37.9	(115 $\mu\text{M}$ )	38.4	(884 $\mu\text{M}$ )	5.7	(884 $\mu\text{M}$ )	[120]
	uric acid	42.0	(103 $\mu\text{M}$ )	18.0	(297 $\mu\text{M}$ )	1.4	(297 $\mu\text{M}$ )	[120]
WDR MoS <sub>2</sub>	urea	63.9	(2 mM)	38.4	(2 mM)	18.4	(2.6 mM)	[123]
	creatinine	66.9	(126 $\mu\text{M}$ )	53.1	(884 $\mu\text{M}$ )	20.4	(884 $\mu\text{M}$ )	[123]
	uric acid	42.7	(133 $\mu\text{M}$ )	23.1	(356 $\mu\text{M}$ )	9.3	(356 $\mu\text{M}$ )	[123]
MoS <sub>2</sub> - CeO <sub>2</sub>	urea	83.7	(2 mM)	59.1	(2 mM)	30.4	(2.6 mM)	[124]
	creatinine	68.8	(126 $\mu\text{M}$ )	53.7	(884 $\mu\text{M}$ )	27.9	(884 $\mu\text{M}$ )	[124]
	uric acid	49.5	(164 $\mu\text{M}$ )	25.1	(356 $\mu\text{M}$ )	14.1	(356 $\mu\text{M}$ )	[124]

In Table 5, a summary of the materials presented in this section is reported to compare their  $q_{eq}$ , i.e. the binding capacity at  $c_{eq}$  towards urea. The materials are ranked according to their  $q_{eq}$  at a concentration of urea equal to 5 mM ( $q_{eq}(c_{eq} = 5\text{mM})$ ). It is worthy to note that different conditions used, e.g. temperature, adsorption media (UTs in DI water, PBS or other buffered solutions, or dialysate spiked with UTs). The impact of ionic strength on the adsorption of the toxins is often non-negligible and, considering the high osmolarity of dialysate, it may affect the results. The sorption coefficient is the ratio of binding capacity to solution concentration, and adsorbent mass is the amount of material needed to adsorb 23.6 g of urea, approximately equivalent to the amount dialysed in a session.

### 2.2.2. Polymers and hydrogels

The focus of this section is on **polymers** and their functionalization strategies to optimize their use as adsorbents for UTs, with a special interest on urea. Particularly, natural polymers offer wide availability, low price and a good degree of biocompatibility; for these reasons, starch, cellulose, and especially chitosan have attracted interest for this application (Figure S4).

**2.2.2.1. Chitosan (CS).** Chitosan is a linear polysaccharide obtained by alkaline deacetylation of chitin, a structural element in the exoskeleton of crustaceans that is biocompatible and biodegradable. The degree of deacetylation (DD) refers to the amount of acetyl groups removed from the chitin structure. The  $\beta$ -(1  $\rightarrow$  4)-linked D-glucosamine (Figure S4a) exposes amine groups with a basic dissociation constant (pKb) value of  $\sim 6$ , which are completely protonated at physiological pH. These amine groups may be used to crosslink the chitosan polymeric chains, with dicarboxylic acids, glutaraldehyde or ions [126]. Chitosan swells considerably in water, forming a hydrogel that can adsorb metals in its structure. The urea molecule has been shown to bind to the unoccupied d-orbital of copper and zinc ions complexed in chitosan, as described by to the bridge and pendant models (Figure S5) [127]. This coordination bond is generally an order of magnitude stronger than the hydrogen bond with water. In particular, copper ( $\text{Cu}^{2+}$ ) is shown to have higher affinity for urea in chitosan compared to other metal ions. In terms of affinity for urea in chitosan, the order of preference among the tested metal ions is as follows:  $\text{Cu}^{2+} \gg \text{Hg}^{2+} > \text{Zn}^{2+} > \text{Cd}^{2+} > \text{Ni}^{2+} > \text{Co}^{2+} \sim \text{Ca}^{2+}$  [20,128]. It is noteworthy that the acceptable concentration of copper in dialysate ( $100 \mu\text{g L}^{-1}$ ) is the highest among this series of metal

ions [129]. For instance, Cu-complexed chitosan (DD 72.47 %, MW 6.5-105), absorbed 120.0 mg/g of urea at a concentration of 21.6 mM, while a porous membrane based on the same material was able to adsorb 78.8 mg/g of urea at 20 mM (with a loading of 40 mg/g of Cu) [130]. The crosslinking may have a strong influence on the adsorption properties of the polymer. A chitosan crosslinked glutaraldehyde (Chi-Glu) copolymer was optimized for urea sorption, with different crosslinking degrees (Glu/Chi weight ratio equal to 0.0835, 0.334, and 0.585) and complexing with copper sulphate (Table 6.1). The  $\text{Cu}^{2+}$  complexed chitosan-glutaraldehyde particles (Glu/Chi 0.585) adsorbed 205.04 mg/g of urea at 10 mM [128,131,132]. In another work, glutaraldehyde-crosslinked chitosan microparticles were reacted sequentially with epichlorohydrin, tetraethylene-pentamine (TEPA) and bromoacetic acid, obtaining a functionalized chitosan named Ac-TEPA-CS (Figure S6). The adsorbent offers pendant groups with four carboxylic groups and four tertiary amines, structurally similar to ethylenediaminetetraacetic acid (EDTA), which is widely known as a metal chelator. The Ac-TEPA-CS particles were complexed with zinc (43.60 mg of Zn over g of polymer) and tested for urea adsorption, capturing 36.8 mg of urea per gram of material (at 17.8 mM) [133] (Table 6.12).

To summarize, adsorption of urea in chitosan is shown to linearly increase, from  $22 \text{ mg g}^{-1}$  to  $78.6 \text{ mg g}^{-1}$ , by increasing the percentage of copper from 4 % wt to 43 % wt in the hydrogel [130]. Reduced molecular weight ( $6.5 \cdot 10^5$  compared to  $10^6$ ) and increased degree of deacetylation (98 % compared to 72 %) appear to promote urea adsorption [123]. The swelling of chitosan (322 % of the pristine chitosan, 150–375 kDa; DD 75 %) can be drastically decreased through crosslinking with glutaraldehyde [128] and by the introduction of copper atoms (72 % swelling in Chi:Glu 1:0.585, complexed with Cu). A greater number of amine (resulting from a higher degree of deacetylation) and a larger amount of copper in the polymer is proven to promote adsorption of urea. [128,130,134]. The selection of a natural molecule as covalent crosslinker, such as genipin, L-aspartic acid, vanillin, instead of glutaraldehyde, can ensure biocompatibility and non-toxicity [126]. However, the release of copper complexed by chitosan still remains an open issue, as the threshold copper concentration in the dialysate is  $100 \mu\text{g L}^{-1}$  [135]. The desorption of copper from chitosan (11.2 % wt of Cu) was shown to be highly influenced by the osmolarity of the solution, with increased osmotic pressure delaying the desorption rate. For example, 18 % of the copper was released in 6 days when exposed to a solution having comparable osmolarity to dialysate [129]. Pathak and Bajpai tested Cu-complexed chitosan for 4 h in a simulated dialysate

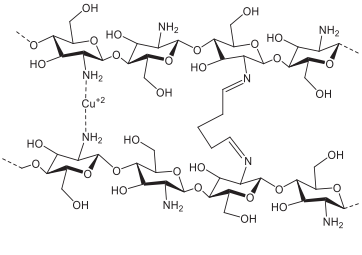
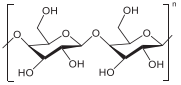
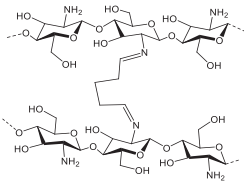
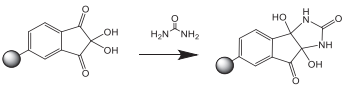
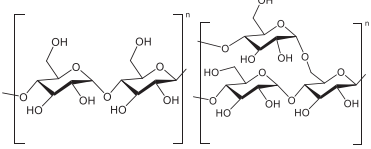
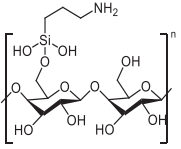
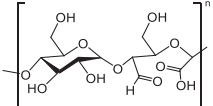
**Table 5**  
Static urea adsorption in nanoporous materials.

	Material	Media	Urea binding capacity $q_{eq}(c_{eq})$		Urea sorption coefficient $\text{mg g}^{-1} \text{mM}^{-1}$	Urea binding capacity at $5\text{mM}q_{eq}(c_{eq} = 5\text{mM})$ $\text{mg g}^{-1}$	Adsorbent mass needed to remove 23.6 g of urea g	Ref.
			$\text{mg g}^{-1}$	(mM)				
MOF	HKUST-1 PAN/PD	DI water	128.0	(2 mM)	64.0	* 320.0	74	[109]
MoS <sub>2</sub>	WDR MoS <sub>2</sub>	DI water	64.0	(2.3 mM)	27.8	* 138.9	170	[123]
Mesoporous silica	SBA-15 NH <sub>2</sub>	PBS pH 7.4	202.0	(20 mM)	10.1	51.0	467	[102]
Mesoporous silica	SBA-15	PBS pH 7.4	119.0	(20 mM)	6.0	29.8	792	[102]
Zeolite	Silicalite (MFI)	DI water	29.0	(7.4 mM)	3.9	19.6	1204	[92]
AC	AC	DI water	8.8	(10 mM)	0.9	4.4	5364	[88]
MXene	Ti <sub>3</sub> C <sub>2</sub> Tx	DI water	13.8	(20 mM)	0.7	3.5	6743	[119]
Zeolite	ZSM-5 (Si/Al 400)	PBS pH 7.4	6.36	(20 mM)	0.3	1.6	14,750	[89]
Zeolite	Mordenite (MOR)	DI water	2.49	(8.5 mM)	0.3	1.5	16,054	[92]

\* data obtained using the extrapolation of the linear regression of the adsorption isotherm.

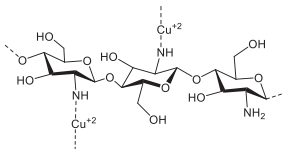
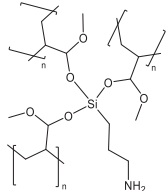
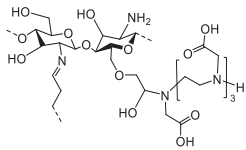


**Table 6**  
Chitosan, cellulose and starch-based materials for urea adsorption.

Material	Chemical structure	Media	Urea binding capacity		Urea sorption coefficient	Urea binding capacity at 5 mM $q_{eq}$ ( $c_{eq} = 5 \text{ mM}$ )	Adsorbent mass needed to remove 23.6 g of urea	Ref.
			$q_{eq}$ ( $c_{eq}$ )	$\text{mg g}^{-1}$				
1 crosslinked chitosan $\text{Cu}^{2+}$ complexed (CP-3)		DI water pH 6 RT	161	(6 mM)	27.0	134.8	175	[128]
		DI water pH 6 RT	205	(10 mM)	20.5		—	
2 ultralight cellulose aerogel		DI water	38.3	(2.3 mM)	16.7	83.3	283	[141]
3 crosslinked chitosan (CP-1)		DI water pH 6 RT	97.2	(6 mM)	16.2	81.0	291	[128]
4 PS nanoparticles ninhydrin groups		dialysate solution 70 °C	126	(20 mM)	6.3	66.9	353	[18]
5 crosslinked chitosan (CP-3)	See row 1	DI water pH 6 RT	98	(10 mM)	9.8	48.9	483	[128]
6 CP-1/Cu(II) (long)	See row 3	DI water	66.4	(9.4 mM)	7.1	35.3	669	[132]
7 Starch nanoparticles		Spent dialysate	45.9	(6.6 mM)	7.0	34.8	678	[138]
8 APTES functionalized cellulose aerogel		DI water	45.3	(7.6 mM)	5.9	29.7	795	[142]
		DI water	27.3	(4.6 mM)	5.9	29.7	795	[142]
9 Oxidized starch nanoparticles (oxy-SNPs)		DI water	33.6	(5.8 mM)	5.8	29.0	814	[139]

(continued on next page)

Table 6 (continued)

Material	Chemical structure	Media	Urea binding capacity $q_{eq}(C_{eq})$  mg g <sup>-1</sup>	Urea sorption coefficient  mM <sup>-1</sup>	Urea binding capacity at 5 mM $q_{eq}(C_{eq} = 5 \text{ mM})$  mg g <sup>-1</sup>	Adsorbent mass needed to remove 23.6 g of urea  g	Ref.
10 Cu <sup>2+</sup> complexed chitosan		PBS pH 7 RT	78.8	(20 mM)	3.9	19.7	1198 [130]
11 Amino-silanized PMMA		DI water	41.7	(20 mM)	2.1	12.82	1841 [143]
12 Zn complexed Ac-TEPA-CS		DI water	36.8	(17.8 mM)	2.1	10.3	2291 [133]

solution, without detecting any leakage of the metal, but this may be attributed to the duration of the experiment and the sensitivity of the detector [136]. The desorption of Zn from Zn-Ac-TEPA-chitosan was investigated for 12 h in a saline solution similar to dialysate (Table S1, without glucose, pH was adjusted to 6.0, 7.0, and 8.0 at 20 °C) without detecting Zn in the elution buffer. A dilute alkali solution (EDTA 0.1 mol L<sup>-1</sup>) was also tested for elution and regeneration; also in this case the amount of Zn immobilized showed no remarkable reduction and the urea adsorption capacity was stable with a decrease of about 4.3 % after 3 cycles [133]. The selling price of commercial chitosan ranges between 16–1000 USD kg<sup>-1</sup>, while when the polymer is crosslinked with glutaraldehyde and complexed with iron it reaches 6130 USD kg<sup>-1</sup> [100].

**2.2.2.2. Starch and cellulose.** Starch is a natural polymer consisting of two main components: amylose (Figure S4b) and amylopectin (Figure S4c). Amylose is a water-soluble linear polymer of D-glucose units, bound with an  $\alpha(1 \rightarrow 4)$  glycosidic bonds, while amylopectin is a water-insoluble branched polymer based on  $\alpha(1 \rightarrow 4)$  glycosidic bonds, but it also contains occasional  $\alpha(1 \rightarrow 6)$  glycosidic bonds [137]. Starch nanoparticles (SNPs) (16.87 % of amylose, MW 4680 kDa, surface area = 4680 m<sup>2</sup> g<sup>-1</sup>) showed superior urea adsorption capacity compared to other forms (flakes or fibre) and other SNPs obtained from different sources, adsorbing 45.9 mg g<sup>-1</sup> of urea at 6.6 mM in patient dialysate (pH 7.4) at 37 °C [138]. Oxidized starch nanoparticles (oxy-SNPs, Table 6.9), prepared via liquid phase oxidation, causing the opening of the heterocycle and resulting in the formation of carboxyl and carbonyl groups, adsorbed 33.6 mg g<sup>-1</sup> of urea at 5.8 mM [139]. However, it is worth noting that oxycelluloses are unstable in dialysate and small fragments of the adsorbent may diffuse back into the bloodstream [20].

Cellulose is a natural polymer made by glucose units bound through a  $\beta(1 \rightarrow 4)$  link (Figure S4d) [140]. An ultralight cellulose aerogel (CA) was tested as urea adsorbent from aqueous solution showing an adsorption capacity for urea of 38.3 mg g<sup>-1</sup> at 2.3 mM [141]. However,

the impact of salt type or other toxins on its adsorption capacity was not studied. An amine-functionalized cellulose aerogel (NCA) was synthesized grafting APTES on the hydroxyl groups (Table 6.2). The adsorption performance was optimized by varying the type of acid and the quantity of APTES (10 mL of APTES for 1 g of CA) reaching an adsorption of 27.29 mg g<sup>-1</sup> at 4.6 mM urea, comparable to the one of pristine chitosan (31.76 mg g<sup>-1</sup> at 5 mM). In addition to the hydroxyl groups NCA adsorption sites, which form hydrogen bonding with urea, the amino and silyl hydroxyl groups introduced through functionalization acted as new adsorption sites, contributing to the improvement of the adsorption performance. Interestingly, the structure of this material bears some structural resemblance to chitosan regarding the presence of amine groups capable of forming hydrogen bonds. However, notable differences exist in the way monomers are linked and the presence of silyl hydroxyl groups [142].

**2.2.2.3. Synthetic polymers.** Polystyrene (PS) nanoparticles functionalized with ninhydrin were incorporated into a polyethersulfone/polyvinylpyrrolidone (PES/PVP) porous polymer matrix. Ninhydrin reacts with amines and the high concentration of urea favours its reaction. Urea adsorption capacities of 66.88 mg g<sup>-1</sup> and 148 mg g<sup>-1</sup>, at concentrations of 5 mM and 30 mM, respectively were observed in static conditions, while in dynamic condition 204 mg g<sup>-1</sup> (30 mM) were adsorbed (Table 6.4). However, despite the satisfactory adsorption capacity, the slow binding kinetics required high temperatures (70 °C) and regeneration of the material was challenging due to the formation of a covalent bond, unless strong acids were employed [18].

Other examples of synthetic polymers are dual-layer hollow fiber membranes prepared using a co-extrusion spinning process, where the inner layer consisted of polysulfone (PSf) tightly bound to the outer layer composed of PSf blended with amino-silanized polymethyl methacrylate (PMMA) (Table 6.11). The amino-silanized PMMA adsorbed urea 2.04 times more than the pristine PMMA [143], however the binding capacity remained relatively small.

**Table 7**  
Summary of the materials simulated for UTs and discussed in Section 2.3.

Class	Material	Target UT(s)	Modelling technique	Ref.
Zeolite	MFI	<i>p</i> -cresol	MC	[155,156]
MOFs	HKUST-1	Urea and creatinine	DFT	[109]
	UiO-66-(COOH) <sub>2</sub> and UiO-66-SO <sub>3</sub> H	Urea and creatinine	DFT	[114]
	Screening of 315 bio-MOFs	Urea and creatinine	MC / MD	[152]
	Screening of 60 bio-MOFs	Urea and creatinine	MC / MD	[152,153]
	Screening of 354 MOFs	Indoxyl sulfate	MC / MD	[157]
COFs	Screening of 433 MOFs	Urea	MC / MD	[154]
	TPA-COF, DAAQ-TFP, DAPH-TFP, Tp-PaSO <sub>3</sub> Li-COF and PHOS-COF (single layers)	Urea	MD / Umbrella sampling / DFT	[158]
	ACA-COF	Creatinine and uric acid	MD	[159]
MXene and C-based materials	Ti <sub>3</sub> C <sub>2</sub> (OH) <sub>2</sub> , Ti <sub>3</sub> C <sub>2</sub> F <sub>2</sub> and Ti <sub>3</sub> C <sub>2</sub> O <sub>2</sub>	Urea and creatinine	DFT	[119,120]
	MXene(Cd, Mn, Cu, Ti, W and Ta)	Urea	MD / Umbrella sampling	[160]
	Graphene, fullerene, carbon nanotubes	Urea	MD / Umbrella sampling	[161–163]
Polymers	Chitosan	Urea and creatinine	DFT	[164]
	Cellulose	Urea	MD	[165]
	Cellulose	Urea	MD	[166]

Table 6 reports the materials described in this chapter, in decreasing order according with their binding capacity for urea at 5 mM, benchmark to represent the operative condition. Since most of the experiments available in the literature were carried out at higher urea concentrations, the adsorption capacity was extracted by linear interpolation of the isotherms to this concentration, assuming all the isotherms linear. The Cu<sup>2+</sup> complexed chitosan-glutaraldehyde CP-3, produced by Wilson and Xue adsorbed 134.8 mg g<sup>-1</sup> of urea at 5 mM [128], proving to be the best material, requiring 175 g of the hydrogel to adsorb the urea dialysed in a session. Swelling of some of the materials presented has to be considered, therefore this swollen polymer will weigh ~ 300 g (considering 72 % of swelling), still an acceptable weight for this application.

### 2.3. Computational modelling of UT sorption

Computational modelling is a promising technique for the screening and the design of materials for a specific application, as it enables the prediction of material properties and the exploration of the underlying mechanisms. For instance, techniques such as density functional theory (DFT) or all-atom simulations have been widely used to verify adsorption of molecules in nanostructured materials and polymers [144,145]. In **molecular simulations** atoms are represented as spheres ruled by a force field (FF) that governs their interactions and constrains their relative motions. The total energy of the system is determined by summing up the various contributions from intra-molecular and inter-molecular interactions, with parameters fine-tuned to accurately reproduce properties measured experimentally. Molecular dynamics (MD) or Monte Carlo (MC) simulations are two widely recognized techniques in molecular simulations, the former based on the integration of the law of motion, the latter based on a statistical approach and a set of arbitrarily imposed moves [146–148]. In the study of adsorption onto a surface, umbrella sampling is often employed as a biased MD method to explore the entire configuration space and calculate the free energy. Among the limitations of all-atom simulations, it is important to mention the neglect of sub-atomic phenomena, like the distortion of electronic density during interactions, a potentially pronounced phenomenon in systems involving transition metals. The intricate nature of metal-coordinated interactions, often involving varying molecular geometries, demands a more detailed description than what all-atom

simulations can provide. In these cases, DFT emerges as a valuable tool, offering a more comprehensive framework for modelling such interactions, by accounting for electron density distributions and molecular geometries with higher accuracy [149–151]. A summary of the simulation works and the relative methodologies used is reported in Table 7.

Key properties for an adsorbent material are the strength of the interaction with the adsorbate, referred as Gibbs free energy of adsorption or binding, and selectivity. Water is often the main competitor for UTs adsorption. Selectivity may be defined as shown in Eq. (2).

$$\alpha_{urea/water}^0 = \frac{S_{urea}^0 D_{urea}^0}{S_{water}^0 D_{water}^0} \quad (2)$$

$S^0$  is the sorption coefficient of adsorbates at infinite dilution,  $D^0$  is the diffusion coefficient of adsorbates at infinite dilution. The product between sorption coefficient ( $S$ ) of adsorbates and diffusion coefficient ( $D$ ) can be used to estimate an effective permeability [152,153]. As the sorption coefficient is associated to the excess chemical potential of the molecule in the sorbent, a sorption-based urea/water selectivity can be estimated as the negative of the difference between the  $\mu^{ex}$  of urea and water  $-(\mu_{urea}^{ex} - \mu_{water}^{ex})$  at infinite dilution in the framework, equivalent to the logarithmic ratio between the sorption constant for urea  $S_{urea}^0$  and for water  $S_{water}^0$ , since  $-(\mu_{urea}^{ex} - \mu_{water}^{ex}) = \rho RT \ln(S_{urea}^0/S_{water}^0)$ , with  $\rho$  the density of the framework [154].

#### 2.3.1. Zeolites

Bergé-Lefranc *et al.* investigated the adsorption of *p*-cresol on the MFI zeolite (silicate, Si/Al  $\infty$ ) through MC simulation [155]. Moreover, they experimentally verified the effect of H<sup>+</sup>, Na<sup>+</sup>, K<sup>+</sup>, Mg<sup>2+</sup> as pairing cations in aluminosilicate MFIs (ZSM-5, Si/Al 30.4) on *p*-cresol capacity adsorption. Two types of adsorption sites were identified in the silicate: one in straight channels and another in zigzag channels. When all available adsorption sites were filled, the theoretical maximum capacity of *p*-cresol molecules adsorbed in the silicate was calculated to be 112 mg g<sup>-1</sup>. However, experimental results showed that only 70 mg g<sup>-1</sup> of *p*-cresol were actually adsorbed from water. This suggests that not all adsorption sites were occupied in practice, as they were already occupied by co-adsorbed water molecules. Subsequent analysis suggested that only two thirds of all possible molecules were in the unit cell of

silicate, resulting in an adsorbed amount of  $75.7 \text{ mg g}^{-1}$ , which closely matched the experimental findings ( $70 \text{ mg g}^{-1}$ ) [155]. Among the samples studied, silicalite exhibited the highest maximum binding capacity, approximately  $70 \text{ mg g}^{-1}$ , with a decreasing trend of silicalite > K-MFI > Na-MFI > Mg-MFI > H-MFI. However, it is worth noting that the target concentration for *p*-cresol is considerably lower than the concentration required to reach such binding capacity. The differences in adsorption mechanisms between pure silica and cation-exchanged MFI samples were related to their hydrophobicity. Silicalite, being hydrophobic, did not need to displace water molecules from the channels to adsorb *p*-cresol. In contrast, cation-exchanged zeolites were hydrophilic and spontaneously filled with water, requiring the displacement of some water molecules for *p*-cresol adsorption. This difference likely contributed to the higher enthalpy of adsorption observed in silicalite [155]. In another study by Wernert *et al.* the adsorption of *p*-cresol within the silicalite was studied with the same methodology. The observed strong affinity of *p*-cresol for silicalite was a result of the hydrophobic interactions in the zeolite. Additionally, the absence of cations in the silicalite channels implied a lack of large, local dipolar moments, rendering the silicalite an overall non-polar structure that interacts with non-polar molecular groups, such as the *p*-cresol methyl group, through attractive hydrophobic interactions [156].

### 2.3.2. Metal organic frameworks (MOFs)

DFT and MC simulations have been used to elucidate sorption mechanisms in MOFs, to confirm the experimental sorption and to screen new MOF structures. DFT calculations have been performed to obtain deeper insight into the adsorption performance of the dual-layer composite nanofiber membrane containing HKUST-1 (grown on PDA/PAN nanofibers and layered with CS/SS nanofibers), presented in Section 2.2.1. According to the adsorption energies reported in Table 8, the binding affinity of urea with HKUST-1 exceeded that of the chitosan sericin (CS/SS) composite, whereas the opposite trend was observed for creatinine. These findings align with the results of adsorption experiments, indicating that in the HKUST-1/PDA/PAN nanofiber membrane, HKUST-1 governed the adsorption of urea molecules, while the CS/SS nanofiber predominantly adsorbed creatinine. The mechanisms underlying the adsorption process involved electrostatic attraction and hydrogen-bonding interactions, with additional contributions from  $\pi$ - $\pi$  stacking interactions. Moreover, both urea and creatinine exhibited hydrogen-bonding, electrostatic, and  $\pi$ - $\pi$  stacking interactions with the CS/SS composite nanofibers [109].

In another DFT study, adsorptions of hippuric and indoxyl sulfate (IS) in molecules of UiO-66 having two different functionalizations ( $-(\text{COOH})_2$ , and  $-\text{HSO}_3$ ) were investigated to compute the free energy of adsorption (Table 8) with the trend matching the experimental isotherms. The two UTs interacted through VdW interactions and  $\pi$ - $\pi$  stacking between the MOFs and the benzene rings of the IS and HA molecules. The enhanced adsorption capability in UiO-66-(COOH)<sub>2</sub> and UiO-66-SO<sub>3</sub>H compared with UiO-66 was attributed to additional Coulombic interactions or hydrogen bonding. In other words, for UiO-66-(COOH)<sub>2</sub> and UiO-66-SO<sub>3</sub>H, the oxygen of Zr-O-C in the MOFs behaved as an H-acceptor (the hydrogen in the carboxyl group of HA and the sulfonic group of IS as the H-donors) and Zr<sub>3</sub>-O-H in the MOFs acted as an H-donor (the oxygen in the carboxyl group of HA and the sulfonic group of IS as the H-acceptors) [114].

**Table 8**

Adsorption Gibbs free energies (kJ/mol) from DFT simulation of urea and creatinine in HKUST-1 and CS/SS [109], hippuric acid and indoxyl sulfate binding in UiO-66, UiO-66-(COOH)<sub>2</sub>, UiO-66-SO<sub>3</sub> [114].

kJ/mol	HKUST-1	CS/SS	UiO-66	UiO-66-(COOH) <sub>2</sub>	UiO-66-SO <sub>3</sub>	
Urea	-149.2	-120.6				[109]
Creatinine	-134.3	-155.4				[109]
Hippuric acid			-73.08	-87.18	-115.25	[114]
Indoxyl sulphate			-286.05	-477.62	-635.66	[114]

These findings unveil the strong impact of functionalization of ligands on UTs adsorption, providing site for hydrogen bonding and  $\pi$ - $\pi$  stacking interactions. Interestingly, synthesis of MOFs allows a flexible strategy to combine different linkers and this results in a dramatically large number of possibilities. For this reason, **computational screenings** emerged as a tool for materials discovery. They are based on a set of techniques ranging from geometrical analysis of the structures (e.g. to understand pore size and surfaces), Grand Canonical MC (GCMC) to measure thermodynamic properties in adsorption of single and multi-component mixtures, such as UT loading, adsorption free energy and enthalpy. In this context the Widom's insertion method [167] represents a valuable methodology to compute infinite dilution properties. MD simulations were also employed to study diffusion in the nanoporous frameworks.

For instance, Yıldız *et al.* carried out a screening using GCMC simulations to predict the adsorption of UTs within 315 bio-MOFs, having biocompatible ligands and metals in the structure [152,153]. In the absence of water molecules, MOF MIL-100 (Fe), showed the highest urea ( $691.9 \text{ mg g}^{-1}$ ) and creatinine ( $730.4 \text{ mg g}^{-1}$ ) uptakes among 60 bio-MOFs (at 310 K and fugacity of UTs equal 1 bar). Moreover, the enthalpy of adsorption,  $\Delta H_{\text{ads}}$ , for creatinine ( $-$ ranging between 24.45 and  $-68.76 \text{ kJ mol}^{-1}$ ) revealed to be lower than that obtained for urea (ranging between  $-17.13$  and  $-46.05 \text{ kJ mol}^{-1}$ ). This confirmed that creatinine was more strongly confined than urea within all 60 bio-MOFs, due to the higher molecular weight and the higher dipole moment. Interestingly, the simulations in mixture conditions carried out on six bio-MOFs showed that:

- (1) compared to single-component conditions, the amount of UTs adsorbed was found to be considerably lower;
- (2) water adsorption in bio-MOFs slightly increased in mixtures, which was attributed to the hydrogen bonds between the UTs and water;
- (3) competition between UTs gains more importance in bio-MOFs with narrow pores, where strong repulsive forces may influence adsorption.

The authors reported that structures based on adenine, dicyanamide and methionine could outperform conventional materials, such as AC or zeolites. Adenine possesses a pyrrole and a pyridine in its structure, resulting in stacking and NH -  $\pi$  interactions between urea and adenine rings and subsequently enhanced intermolecular interactions [152,153].

Palabiyık *et al.* investigated urea and creatinine adsorption of 60 bio-MOFs using a similar methodology, in addition to the study of transport properties. OREZES, a methionine-based MOF, displayed the highest selectivity  $S^0_{\text{urea/water}}$  (348) for urea/water separation at infinite dilution (310 K), followed by BEPIX (313, amino-based) and KEXDIB (148, based on dicyanamide). Interestingly, BEPIX exhibited the highest creatinine/water selectivity ( $1.5 \times 10^5$ ) under the same conditions, followed by KEXDIB. Furthermore, the research highlighted the competitive effects between UTs in binary or ternary mixtures. Specifically, while creatinine permeability in bio-MOFs increased, the urea permeability decreased in ternary mixture conditions. Furthermore, VdW interactions appeared significantly stronger than Coulombic. On the other hand, electrostatic energy between adsorbate molecules

played a crucial role in water diffusion, due to the formation of strong hydrogen bonds between water molecules [152,153]. It is worth noting that in both works, the concentrations of UTs might be far from the real HD condition, but they still provide a useful insight on a large set of frameworks.

A similar approach was applied to shortlist six among 354 MOFs, with high uptakes of indoxyl sulfate using MC simulations. The adsorption performance of MOFs was shown to be a complex interplay of geometrical descriptors (e.g. available surface area and void fraction) and thermodynamic parameters (Henry's coefficient of water). Six MOFs were revealed to have an uptake higher than 2100 mg g<sup>-1</sup>. Both carboxylic groups and the pyrrolidinyll nitrogen atom, as well as metal clusters, enhanced the adsorption of indoxyl sulfate [157].

### 2.3.3. Covalent organic frameworks (COFs)

Organic frameworks may be built only by organic ligands, obtaining the so-called covalent organic frameworks (COFs). COFs are endowed with high stability in water, even in the presence of electrolytes and at extreme conditions of pH, due to the strong covalent bonds between their units. To the best of our knowledge, there are no experimental works testing these materials for urea removal. 433 COFs from CoreCOF database [168] were screened for urea showing the impact of functionalization on the excess chemical potential ( $\mu^{ex}$ ), measured at infinite dilution through the Widom's insertion method. The  $\mu_{urea}^{ex}$  was calculated to evaluate the urea binding strength in COFs. The adsorption performance was measured in terms of excess chemical potential of urea  $\mu_{urea}^{ex}$  and the selectivity with respect to water  $\mu_{urea}^{ex} - \mu_{water}^{ex}$  at 310 K. Despite structural parameters did not correlate with material performance, COFs containing fluorine, a highly electronegative atom, were shown to be the best COFs for selective urea binding at infinite dilution. Particularly, COF-F6 was the one displaying stronger interactions with urea, thanks to the highly fluorinated alkyl chains ( $\mu_{urea}^{ex}$  in the range of -27.8 to -6.2 kJ/mol for the methoxy, propoxy, allyloxy grafting of the pristine TF-DHz COFs reaches -84.2 kJ/mol for COF-F6) [154].

Jahromi et al. compared the adsorption of urea on single layers of 5 COFs (TPA-COF, DAAQ-TFP, DAPH-TFP, Tp-PaSO<sub>3</sub>Li-COF, and of PHOS-COF) in a urea/water mixture with an initial concentration of 170 mM through MD simulation [158]. In this case, COFs were modelled as nanosheets, with a dramatic difference with respect to the cavities. The adsorption surface exposed is different, therefore the binding sites and the binding mechanisms may significantly differ. The free energies were calculated through the umbrella sampling method. TPA-COF (-29 kJ mol<sup>-1</sup>) showed the lowest Gibbs free energy of adsorption, mostly driven by the highest number of hydrogen bonds created between TPA-COF and urea molecules. According to DFT calculations, hydroxylation of TPA-COF further improved the adsorption process through attractive interaction between the electronegative -OH group and the amine functional group of the urea molecule.

Creatinine and uric acid adsorption on a cationic azacalix-4-arene-based COF (ACA-COF), were verified experimentally and theoretically by Skorjanc and coworkers [159]. Results from MD simulations showed that uric acid exhibits a higher affinity than creatinine onto ACA-COF, with an average removal capacity of 86 % from an aqueous uric acid solution. In contrast, the removal capacity for creatinine was found to be approximately 22 %. The selectivity toward uric acid showed agreement with experimental results. The positively charged nitrogen atoms of the COFs confirmed to bind with uric acid, in its dissociated form, primarily through electrostatic forces. Additionally, uric acid binds between adjacent aromatic rings with -NH<sub>2</sub>, forming a  $\pi$ - $\pi$  stacking interaction. In contrast, the aromatic ring containing two NO<sub>2</sub> groups is the least favoured region for uric acid binding due to its negative partial charge localized at the polar NO<sub>2</sub> groups causing repulsive interactions [159].

### 2.3.4. Mxenes and C-based materials

MXenes and 2D layered inorganic materials were tested

experimentally for urea sorption. Additionally, DFT calculations were used to obtain deeper insight into the adsorption of UTs onto MXenes, to support the experimental results. Simulations revealed that urea adsorbs between intercalating stacked sheets, preferentially in the parallel-to-surface conformation, regardless of surface terminations. The -OH- terminal surfaces exhibited the most stable adsorption state for urea, with binding energies of -89.73 kJ mol<sup>-1</sup>. This trend was followed by -O- and -F- terminated surfaces [119]. Creatinine adsorption followed the same trend for Ti<sub>3</sub>C<sub>2</sub>(OH)<sub>2</sub> (-115.8 kJ mol<sup>-1</sup>), Ti<sub>3</sub>C<sub>2</sub>F<sub>2</sub> (-68.5 kJ mol<sup>-1</sup>) and Ti<sub>3</sub>C<sub>2</sub>O<sub>2</sub> (-94.55 kJ mol<sup>-1</sup>). The enhanced stability of creatinine on the Ti<sub>3</sub>C<sub>2</sub>(OH)<sub>2</sub> surface was supported by the increased charge transfer between creatinine and the Ti<sub>3</sub>C<sub>2</sub>(OH)<sub>2</sub> surface [120].

MD calculations were used to compare the adsorption performance of Cd, Mn, Cu, Ti, W, and Ta based MXenes (Cd<sub>2</sub>C, Mn<sub>2</sub>C, Cu<sub>2</sub>C, Ti<sub>2</sub>C, W<sub>2</sub>C, and Ta<sub>2</sub>C) using the all-atom optimized potential for liquid simulations (OPLS-AA) force field. VdW forces were shown to dominate non-bonded interactions between MXenes and urea. Moreover, the lowest Gibbs free energy of adsorption equivalent to -42.32 kJ mol<sup>-1</sup> was observed for Cd<sub>2</sub>C, which represented the best candidate for urea removal in comparison with other MXenes [160].

Other nanostructured materials such as graphene, carbon nanotube and fullerenes were studied computationally using the same methodology and force field. The Gibbs free energies of adsorption for urea obtained from MD simulations, through applying umbrella sampling, are reported in Table 9. Among nitrogen and phosphorus doped-graphenes, graphene with 10 % nitrogen was optimal for urea adsorption, minimizing the Gibbs free energy at -11.5 kJ mol<sup>-1</sup> (-5.9 kJ mol<sup>-1</sup> difference with pristine graphene) [161]. Similarly, adsorption of urea on fullerene with 8 % nitrogen doping revealed the lowest Gibbs free energy among the simulated doping concentrations, equal to -22.49 kJ mol<sup>-1</sup> (-15.41 kJ mol<sup>-1</sup> difference with pristine fullerene). However, the boron-carbon-nitride nanotube containing 24 % of each boron and nitrogen showed the highest urea adsorption (71.25 %) compared to pristine graphene, carbon nanotubes, and boron-carbon-nitride nanolayers in urea concentrations of 684 mM. The Gibbs free energy of adsorption was -24.82 kJ mol<sup>-1</sup> [163].

### 2.3.5. Polymers

Nanoporous materials often possess a crystalline and stable structure, resulting in fewer conformational states and enabling a more computationally-effective characterization of their cavities. Polymers contain numerous conformational states and their structures are typically amorphous, necessitating simulations with a large number of atoms. Most studies model the adsorption of UTs on a monomer or on a single polymeric chain containing small number of monomers. Also, some simulations were run at a concentration of urea in solution higher than in spent dialysate, therefore binding capacities cannot be compared

**Table 9**  
Gibbs free energy ( $\Delta G_b$ , kJ/mol) of adsorption of urea on Carbon nanostructured materials using MD simulation [161–163].

Material	C	P	N	B	H	$\Delta G_b$	Ref.
Graphene	50 %	50 %	–	–	–	-6.7	[161]
	85 %	–	15 %	–	–	-8.1	
	90 %	–	10 %	–	–	-11.5	
	100 %	–	–	–	–	-5.6	
Fullerene	50 %	50 %	–	–	–	-17.9	[162]
	75 %	–	25 %	–	–	-8.5	
	92 %	–	8 %	–	–	-22.5	
	100 %	–	–	–	–	-7.1	
BCN-nanotube	49 %	–	24 %	24 %	2 %	-24.8	[163]
BCN-nanolayer	25 %	–	50 %	26 %	–	-22.9	
Graphene	100 %	–	–	–	–	-19.3	
Carbon nanotube	100 %	–	–	–	–	-18.0	

with experiments, but modelling results offer relevant molecular insight on the sorption mechanism.

The adsorption of urea and creatinine on a chitosan monomer was investigated through DFT simulations: the interaction energies of chitosan-creatinine and chitosan-urea complexes were in the range of  $-16.7 \text{ kJ mol}^{-1}$  and  $-83.7 \text{ kJ mol}^{-1}$  which were classified as a medium hydrogen bond interactions. Creatinine is an electrophilic species, that showed enhanced interaction with chitosan due to the hydrogen bonds with chitosan, stronger than those formed by urea. The interaction of hydroxyl groups in the polymer with the nitrogen atoms of creatinine, results in a binding energy of  $-54.4 \text{ kJ mol}^{-1}$  [164]. In another computational study, urea adsorption (19.76 % wt) on a single chain of cellulose containing (4.0 % wt) in aqueous solution, (330 mM), was simulated by Cai *et al.* Hydrogen bonding was the dominant mechanism, in which oxygen atoms of urea behaved as proton-acceptors and hydroxyl hydrogen atoms of cellulose as proton donors [165]. To determine various thermodynamic contributions associated with urea adsorption on cellulose at urea concentration of 166 and 5000 mM, MD simulations were performed by Chen *et al* [166]. Urea dissolution in water is known as an endothermic process ( $\Delta H^0 = +15.31 \text{ kJ mol}^{-1}$  [169]) due to the weaker nature of the newly formed urea – water hydrogen bonds compared to the disrupted water – water hydrogen bonds. Therefore, this phenomenon is driven by entropy. MD results for adsorption of urea on cellulose from aqueous solution showed that regardless of concentration, almost 5 % of the dissolved urea molecules were adsorbed on the cellulose surface. Electrostatic interactions accounted for nearly two-thirds of the total interaction energy. However, the driving force of urea accumulation near the cellulose surface appeared to be the result of London dispersion forces rather than electrostatic interactions. This can be attributed to the weaker nature of urea – cellulose hydrogen bonds compared to urea – water hydrogen bonds, as the partial charges of the hydroxyl groups of cellulose are smaller than those of water. Urea adsorption on cellulose results in the expulsion of 2.2-2.5 water molecules from the first adsorption shell, which are partially confined from the polymer surface to the bulk, leading to an increase in the entropy of the expelled water. This process also affects the bulk water entropy; consequently, the net solvent entropy change is always positive, as the entropy of urea adsorbed on the cellulose surface is consistently lower than the increase in the entropy of water, thereby facilitating urea adsorption on cellulose [166].

### 3. Conclusions

Hemodialysis represents the most established technique for renal replacement therapy. The hurdles of HD are the disruption to the lifestyle of ESRD patients and large water consumption. Miniaturization, portability, delivery and accessibility of HD are key points addressed by the clinical and engineering community to overcome the drawbacks of the treatment, aiming at the design of portable and wearable devices, to provide a continuous and home-delivered HD. In particular, the regeneration of spent dialysate would reduce the amount of water required, making the treatment more accessible and portable. In addition, a new, clinically-oriented classification of uremic toxins brings into the picture other target molecules alongside urea that, despite their low concentration in blood, may have an important role in the uremic syndrome experienced by dialysed patients.

New approaches to urea removal, other than the enzymatic conversion, have been proposed, such as photoelectrochemical techniques, that offer low power consumption and effectiveness in urea decomposition, are limited to the generation of by-products and low selectivity. A system including a forward osmosis and activated carbon to capture residual by-products has been proposed to prevent these drawbacks. FO membranes offer an opportunity for reduction of water consumption, but they are not suitable for the design of a portable or wearable device since they present limitations in urea rejection and are burdened by membrane fouling.

Adsorption represents a promising alternative for urea removal. Conventional materials, such as AC and zeolites have low urea binding capacity, but may be used to remove other organic UTs from the spent dialysate. Among nanostructured materials, new organic frameworks such as the HKUST-1/PDA/PAN nanofiber membrane and CS/SS [109], MoS<sub>2</sub> with widened interlayer spacing [123] or amine functionalized mesoporous silica SBA-15 NH<sub>2</sub> [102] showed remarkable adsorption capacities, requiring less than 500 g of adsorbent to keep the urea concentration at non-CKD levels. However, the stability of these adsorbents in dialysate represents an important point to be addressed. Polymers are an attractive class of materials for sorption of UTs, specifically chitosan when complexed with copper [128] appears to have the highest adsorption ( $134.8 \text{ mg g}^{-1}$  at 5 mM). Interestingly, the presence of transition metals, such as copper, in the hydrogels to promote urea binding, but it could represent a safety issue. Cellulose aerogels are another interesting material for urea sorption [141].

It is important to remark upon the lack of a harmonized and consistent methodology of testing, in terms of temperature, media and concentrations of uremic toxins, which makes comparison of materials more challenging. For instance, deionized water or phosphate buffer solutions are often preferred over mock spent-dialysate solutions which include additional components and other dialysed species (e.g. ions, glucose, amino acids) that may generate competition from other UTs. More importantly, stability in a buffer solution and biocompatibility of adsorbents represent key points seldom addressed. For this reason, in our opinion, adsorption of materials should be measured in mock spent-dialysate solutions, in a range of equilibrium concentrations compatible with the target concentration of each UT in blood; not least, adsorption data should present binding capacities along with equilibrium concentrations, providing a consistent performance indicator of the materials, conversely from removal efficiencies or initial concentrations.

Molecular modelling of materials appears a valuable tool to explore binding mechanisms, predicting and optimizing of material properties. For instance, the study of *p*-cresol in MFI zeolites or the adsorption of urea and creatinine in UiO-66, HKUST-1, UiO-66 type MOFs and Ti<sub>3</sub>C<sub>2</sub>T<sub>x</sub> MXenes showed good agreement with the experimental findings, unveiling the mechanism ruling the adsorption of UTs and providing information about the quality of interactions. The study of free energy of binding in 2-D layer materials showed the impact of doping and functionalization of graphene, fullerenes, MXenes and COFs. For instance, both graphene and fullerene have an optimal doping of nitrogen (comprising between 8–10 %) that maximizes the urea binding energy. The use of molecular modelling to investigate the behaviour of nanoporous materials and polymers has been the objective of several works, providing details on the mechanism of sorption or aiding the optimization by changing functional groups. Molecular simulations are also used to assess the performance and screen large libraries of MOFs and COFs for this application. Such methodology aims at accelerating and optimizing the design of organic frameworks and it showed the importance of solvation and mixture effects, addressed in the adsorption of urea, creatinine and indoxyl sulphate.

In conclusion, material science can actively employ the potential of experimental testing and molecular modelling to design adsorbents for uremic toxins capture. UTs adsorption from spent dialysate emerges as a promising enabling technology for dialysate regeneration and the development of a portable or wearable artificial kidney, to minimize the water consumption and alleviate the lifestyle disruption and uremic syndrome of ESRD patients.

### Declaration of competing interest

The authors declare that they have no known competing financial interests or personal relationships that could have appeared to influence the work reported in this paper.

## Acknowledgments

This work was supported by Kidney Research UK through the programs Kidney Medtech Competition Award 2022 and Kidney Research UK – Stonegate Research Project Grant SG\_KS\_RP\_012\_20221129. We also acknowledge financial support from the Royal Society of Edinburgh (RSE) through RSE Scottish Government SAPHIRE Grant: 2022 (Funder reference number 2816). The School of Engineering of Edinburgh has supported the PhD scholarship of Mr. Thomas Fabiani.

## Appendix A. Supplementary data

Supplementary data to this article can be found online at <https://doi.org/10.1016/j.seppur.2024.130776>.

## Data availability

Data will be made available on request.

## References

- [1] C. Ronco, W.R. Clark, Haemodialysis membranes, *Nat. Rev. Nephrol.* 14 (2018) 394–410, <https://doi.org/10.1038/s41581-018-0002-x>.
- [2] W.G. Couser, G. Remuzzi, S. Mendis, M. Tonelli, The contribution of chronic kidney disease to the global burden of major noncommunicable diseases, *Kidney Int.* 80 (2011) 1258–1270, <https://doi.org/10.1038/ki.2011.368>.
- [3] J.Y. Yeun, B. Young, T.A. Depner, A.A. Chin, Hemodialysis, in: *Brenner's Textbook of Nephrology*, 2020, pp. 2038–2093.
- [4] B.A. Boerstra, R. Boenink, M.E. Astley, M. Bonthuis, S. Abd ElHafeez, F. Arribas Monzón, A. Åsberg, P. Beckerman, S. Bell, A. Cases Amenós, P. Castro de la Nuez, M.A.G.J. ten Dam, A. Debska-Slizien, N. Gjorgjievski, R. Giudotti, J. Helve, K. Hommel, A. Idrizi, Ó.S. Iridriáson, F. Jarraya, J. Kerschbaum, K. S. Komissarov, N. Kozliuk, M. Kravljaca, M. Lassalle, J.M. De Meester, M. Ots-Rosenberg, Z. Plummer, D. Radunovic, O. Razvazhaieva, H. Resic, O.L. Rodríguez Arévalo, C. Santieste de Pablos, N. Seyahi, M.F. Slon-Roblero, M. Stendahl, M. Tolaj-Avdiu, S. Trujillo-Alemán, I. Ziedina, E. Ziginskiene, A. Ortiz, K.J. Jager, V.S. Stel, A. Kramer, The ERA Registry Annual Report 20\*21: a summary, *Clin. Kidney J.* 17 (2024) sfad281, <https://doi.org/10.1093/cjk/sfad281>.
- [5] H. Htay, A.K. Bello, A. Levin, M. Lunney, M.A. Osman, F. Ye, G.E. Ashuntang, E. Bellorin-Font, M.B. Gharbi, S.N. Davison, M. Ghnaimat, P. Harden, V. Jha, K. Kalantar-Zadeh, P.G. Kerr, S. Klarenbach, C.P. Kovesdy, V.A. Luyckx, B. Neuen, D. O'Donoghue, S. Ossareh, J. Perl, H.U. Rashid, E. Rondeau, E.J. See, S. Saad, L. Sola, I. Tchokhonelidze, V. Tesar, K. Tungsanga, R.T. Kazancioglu, A. Yee-Moon Wang, C.-W. Yang, A. Zemchenkov, M. Zhao, K.J. Jager, F.J. Caskey, V. Perkovic, K.K. Jindal, I.G. Okpechi, M. Tonelli, D.C. Harris, D.W. Johnson, Hemodialysis Use and Practice Patterns: An International Survey Study, *Am. J. Kidney Dis.* 77 (2021) 326–335.e1, <https://doi.org/10.1053/j.ajkd.2020.05.030>.
- [6] I. Ledebó, P.-J. Blankestijn, Haemodialysis—optimal efficiency and safety, *NDT Plus* 3 (2010) 8–16, <https://doi.org/10.1093/ndtplus/sfp149>.
- [7] J.H. Lawson, L.E. Niklason, P. Roy-Chaudhury, Challenges and novel therapies for vascular access in haemodialysis, *Nat. Rev. Nephrol.* 16 (2020) 586–602, <https://doi.org/10.1038/s41581-020-0333-2>.
- [8] G. De Simone, A. di Masi, P. Ascenzi, Serum Albumin: A Multifaceted Enzyme, *Int. J. Mol. Sci.* 22 (2021) 10086, <https://doi.org/10.3390/ijms221810086>.
- [9] K. Oshvandi, R. Kavyanesh, S.R. Borzuo, M. Gholyaf, High-Flux and Low-Flux Membranes: Efficacy in Hemodialysis, *Nurs. Midwifery Stud.* 3 (2014) e21764.
- [10] J.K. Leyboldt, A.K. Cheung, Removal of high-molecular-weight solutes during high-efficiency and high-flux haemodialysis, *Nephrol. Dial. Transplant.* 11 (1996) 329–335, <https://doi.org/10.1093/ndt/11.2.329>.
- [11] J. Vienken, Membranes for haemodialysis. What is more important, sieving coefficient or flux?, *Probl. Eksploat.* (2013) 7–16.
- [12] Comprehensive Membrane Science and Engineering, ScienceDirect (n.d.). <http://www.sciencedirect.com/5070/referencework/9780080932507/comprehensive-membrane-science-and-engineering> (accessed September 9, 2024).
- [13] M.Y. Jaffrin, L.H. Ding, J.M. Laurent, Simultaneous convective and diffusive mass transfers in a hemodialyzer, *J. Biomech. Eng.* 112 (1990) 212–219, <https://doi.org/10.1115/1.2891174>.
- [14] S. Ahmad, *Manual of Clinical Dialysis*, 2nd ed, 2009 edition, Springer, 2014.
- [15] S.K. Bowry, C. Chazot, The scientific principles and technological determinants of haemodialysis membranes, *Clin. Kidney J.* 14 (2021) i5–i16, <https://doi.org/10.1093/cjk/sfab184>.
- [16] A.T. Azar, B. Canaud, Hemodialysis System, in: *Model. Control Dial. Syst.*, Springer Berlin Heidelberg, Berlin, Heidelberg, 2013, pp. 99–166, [https://doi.org/10.1007/978-3-642-27458-9\\_3](https://doi.org/10.1007/978-3-642-27458-9_3).
- [17] M.K. van Gelder, S.M. Mihaila, J. Jansen, M. Wester, M.C. Verhaar, J.A. Joles, D. Stamatialis, R. Masereeuw, K.G.F. Gerritsen, From portable dialysis to a bioengineered kidney, *Expert Rev. Med. Devices* 15 (2018) 323–336, <https://doi.org/10.1080/17434440.2018.1462697>.
- [18] I. Geremia, J.A.W. Jong, C.F. van Nostrum, W.E. Hennink, K.G.F. Gerritsen, D. Stamatialis, New mixed matrix membrane for the removal of urea from dialysate solution, *Sep. Purif. Technol.* 277 (2021) 119408, <https://doi.org/10.1016/j.seppur.2021.119408>.
- [19] ANSI/AAMI RD62:2006, Water Treat. Equip. Hemodial. Appl. (2006). <https://webstore.ansi.org/standards/aami/ansiaamir622006a12009rd62> (accessed September 9, 2024).
- [20] M.K. van Gelder, J.A.W. Jong, L. Folkertsma, Y. Guo, C. Blüchel, M.C. Verhaar, M. Odijk, C.F. Van Nostrum, W.E. Hennink, K.G.F. Gerritsen, Urea removal strategies for dialysate regeneration in a wearable artificial kidney, *Biomaterials* 234 (2020) 119735, <https://doi.org/10.1016/j.biomaterials.2019.119735>.
- [21] C.S. Hanson, J.R. Chapman, J.C. Craig, D.C. Harris, L.K. Kairaitis, M. Nicdao, M. Mikaheal, A. Tong, Patient experiences of training and transition to home haemodialysis: A mixed-methods study, *Nephrology* 22 (2017) 631–641, <https://doi.org/10.1111/nep.12827>.
- [22] R. M. Klevens, J.R. Edwards, M.L. Andrus, K.D. Peterson, M.A. Dudeck, T. C. Horan, Dialysis Surveillance Report: National Healthcare Safety Network (NHSN)-data summary for 2006, *Semin Dial.* 21 (2008) 24–28, <https://doi.org/10.1111/j.1525-139x.2007.00379.x>.
- [23] M.B. Rivara, J. Himmelfarb, From Home to Wearable Hemodialysis: Barriers, Progress, and Opportunities, *Clin. J. Am. Soc. Nephrol.* (2024), <https://doi.org/10.2215/CJN.0000000000000424>.
- [24] S. Alloati, A. Molino, M. Manes, G. Bonfant, V. Pellu, Long Nocturnal Dialysis, *Blood Purif.* 20 (2003) 525–530, <https://doi.org/10.1159/000069555>.
- [25] P.G. Kerr, K.R. Polkinghorne, S.P. McDonald, Home hemodialysis in Australia: Current perspective, *Hemodial. Int.* 12 (2008) S6–S10, <https://doi.org/10.1111/j.1542-4758.2008.00288.x>.
- [26] A. Chedid, D.H. Knicely, Overview of Benefits and Limitations of Home Hemodialysis, in: D.H. Knicely, E.M. Abdel-Rahman, K.I. Greenberg (Eds.), *Handb. Home Hemodial.*, McGraw Hill, New York, NY, 2021.
- [27] J.W.M. Agar, Home hemodialysis in Australia and New Zealand: Practical problems and solutions, *Hemodial. Int.* 12 (2008) S26–S32, <https://doi.org/10.1111/j.1542-4758.2008.00292.x>.
- [28] Home Dialysis Energy Reimbursement in Scotland, *Kidney Care UK* (n.d.). <https://www.kidneycareuk.org/about-kidney-health/living-kidney-disease/home-dialysis-energy-reimbursement-scotland/> (accessed September 9, 2024).
- [29] Home hemodialysis Fresenius, Fresenius Med. Care (2023). <https://www.freseniusmedicalcare.com/en/home-hemodialysis-overview> (accessed September 9, 2024).
- [30] Quanta, Quanta, Quanta (2023). <https://dev-uk-quanta-web2.azurewebsites.net/> (accessed September 9, 2024).
- [31] T.W. Ferguson, G.D. Harper, J.E. Milad, P.V.J. Komenda, Cost of the quanta SC+ hemodialysis system for self-care in the United Kingdom, *Hemodial. Int.* 26 (2022) 287–294, <https://doi.org/10.1111/hdi.12994>.
- [32] Outset Medical | Tablo Hemodialysis System, (n.d.). <https://www.outsetmedical.com/tablo/> (accessed September 9, 2024).
- [33] S.E. Young, L.J. Khoshnaw, R.J. Johnson, Climate and the Nephrologist: The Intersection of Climate Change, Kidney Disease, and Clinical Care, *Clin. J. Am. Soc. Nephrol.* 18 (2023) 411, <https://doi.org/10.2215/CJN.08530722>.
- [34] N. Neirynek, R. de Smet, E. Schepers, R. Vanholder, G. Glorieux, Classification and a List of Uremic Toxins, in: *Urem. Toxins*, John Wiley & Sons Inc, Hoboken, NJ, USA, 2012, pp. 13–33, <https://doi.org/10.1002/9781118424032.ch2>.
- [35] S.K. Bowry, P. Kotanko, R. Himmele, X. Tao, M. Anger, The membrane perspective of uraemic toxins: which ones should, or can, be removed? *Clin. Kidney J.* 14 (2021) i17–i31, <https://doi.org/10.1093/cjk/sfab202>.
- [36] T. Niwa, Recent progress in the analysis of uremic toxins by mass spectrometry, *J. Chromatogr. B* 877 (2009) 2600–2606, <https://doi.org/10.1016/j.jchromb.2008.11.032>.
- [37] M.H. Rosner, T. Reis, F. Husain-Syed, R. Vanholder, C. Hutchison, P. Stenvinkel, P.-J. Blankestijn, M. Cozzolino, L. Juillard, K. Kashani, M. Kaushik, H. Kawanishi, Z. Massy, T.L. Sirich, L. Zuo, C. Ronco, Classification of Uremic Toxins and Their Role in Kidney Failure, *Clin. J. Am. Soc. Nephrol.* 16 (2021) 1918, <https://doi.org/10.2215/CJN.02660221>.
- [38] R. Vanholder, R. De Smet, G. Glorieux, A. Argilés, U. Baurmeister, P. Brunet, W. Clark, G. Cohen, P.P. De Deyn, R. Deppisch, B. Descamps-Latscha, T. Henle, A. Jörres, H.D. Lemke, Z.A. Massy, J. Passlick-Deetjen, M. Rodriguez, B. Stegmayr, P. Stenvinkel, C. Tetta, C. Wanner, W. Zidek, For the European Uremic Toxin Work Group (EUTox), Review on uremic toxins: Classification, concentration, and interindividual variability, *Kidney Int.* 63 (2003) 1934–1943, <https://doi.org/10.1046/j.1523-1755.2003.00924.x>.
- [39] S.K. Bowry, F. Kircelli, M. Nandakumar, T.J. Vachharajani, Clinical relevance of abstruse transport phenomena in haemodialysis, *Clin. Kidney J.* 14 (2021) i85–i97, <https://doi.org/10.1093/cjk/sfab183>.
- [40] G. Shao, H. Tang, S. Ren, S.A. Creason, S. Faisal, A. Galperin, A. Aliseda, D. Gao, B. Ratner, B.J. Hinds, Dialysate regeneration via urea photodecomposition with TiO<sub>2</sub> nanowires at therapeutic rates, *Artif. Organs N/a* (2023), <https://doi.org/10.1111/aor.14514>.
- [41] J.D. Pittard, Chapter 13 - Safety Monitors in Hemodialysis, in: A.R. Nissenson, R. N. Fine (Eds.), *Handb. Dial. Ther.*, Fifth Ed., Elsevier, 2017, pp. 162–190, <https://doi.org/10.1016/B978-0-323-39154-2.00013-8>.
- [42] J.T. Olesberg, M.A. Arnold, M.J. Flanagan, Online Measurement of Urea Concentration in Spent Dialysate during Hemodialysis, *Clin. Chem.* 50 (2004) 175–181, <https://doi.org/10.1373/clinchem.2003.025569>.
- [43] The European Uremic Toxins (EUTox) Database, (2023). [www.uremic-toxins.org](http://www.uremic-toxins.org) (accessed September 9, 2024).
- [44] R. Vanholder, S. Van Laecke, G. Glorieux, What is new in uremic toxicity? *Pediatr. Nephrol. Berl. Ger.* 23 (2008) 1211–1221, <https://doi.org/10.1007/s00467-008-0762-9>.

- [45] I.D. Weiner, W.E. Mitch, J.M. Sands, Urea and ammonia metabolism and the control of renal nitrogen excretion, *Clin. J. Am. Soc. Nephrol.* 10 (2015) 1444–1458, <https://doi.org/10.2215/CJN.10311013>.
- [46] A.O. Hosten, BUN and Creatinine, in: H.K. Walker, W.D. Hall, J.W. Hurst (Eds.), *Clin. Methods Hist. Phys. Lab. Exam*, 3rd ed., Butterworths, Boston, 1990.
- [47] R.A. Pollock, G.Y. Gor, B.R. Walsh, J. Fry, I.T. Ghampson, Y.B. Melnichenko, H. Kaiser, W.J. DeSisto, M.C. Wheeler, B.G. Frederick, Role of Liquid vs Vapor Water in the Hydrothermal Degradation of SBA-15, *J. Phys. Chem. C* 116 (2012) 22802–22814, <https://doi.org/10.1021/jp303150e>.
- [48] M. D'Apollito, X. Du, H. Zong, A. Catucci, L. Maiuri, T. Trivisano, M. Pettoello-Mantovani, A. Campanozzi, V. Raia, J.E. Pessin, M. Brownlee, I. Giardino, Urea-induced ROS generation causes insulin resistance in mice with chronic renal failure, *J. Clin. Invest.* 120 (2010) 203–213, <https://doi.org/10.1172/JCI37672>.
- [49] W.L. Lau, N.D. Vaziri, Urea, a true uremic toxin: the empire strikes back, *Clin. Sci.* 131 (2016) 3–12, <https://doi.org/10.1042/CS20160203>.
- [50] I. Giardino, M. D'Apollito, M. Brownlee, A.B. Maffione, A.L. Colia, M. Sacco, P. Ferrara, M. Pettoello-Mantovani, Vascular toxicity of urea, a new “old player” in the pathogenesis of chronic renal failure induced cardiovascular diseases, *Turk. Arch. Pediatr. Pediatr. Arş.* 52 (2017) 187–193, <https://doi.org/10.5152/TurkPediatriArs.2017.6314>.
- [51] R. Vanholder, T. Gryp, G. Glorieux, Urea and chronic kidney disease: the comeback of the century? (in uraemia research), *Nephrol. Dial. Transplant.* 33 (2018) 4–12, <https://doi.org/10.1093/ndt/gfx039>.
- [52] V. Verdier, C.O. Soulage, L. Koppe, New clinical evidence for urea toxicity, *Nephrol. Dial. Transplant.* 37 (2022) 1–4, <https://doi.org/10.1093/ndt/gfab269>.
- [53] G. Shao, H. Tang, S. Ren, S.A. Creason, D. Gao, B.D. Ratner, B.J. Hinds, Dialysate Regeneration with Urea Selective Membrane Coupled to Photoelectrochemical Oxidation System (Adv. Mater. Interfaces 13/2022), *Adv. Mater. Interfaces* 9 (2022) 2270070, <https://doi.org/10.1002/admi.202270070>.
- [54] T. Niwa, Update of uremic toxin research by mass spectrometry, *Mass Spectrom. Rev.* 30 (2011) 510–521, <https://doi.org/10.1002/mas.20323>.
- [55] X. Qi, Y. Zhang, J. Gao, T. Chen, A. Zhao, Y. Yan, W. Jia, Metabolite profiling of hemodialysate using gas chromatography time-of-flight mass spectrometry, *J. Pharm. Biomed. Anal.* 55 (2011) 1142–1147, <https://doi.org/10.1016/j.jpba.2011.04.001>.
- [56] K. Kashani, M.G. Cozzolino, Z.A. Massy, P.J. Blankestijn, P. Stenvinkel, M. H. Rosner, C. Ronco, Proposal for a New Classification of Solutes of Interest in Uremia and Hemodialysis, *Blood Purif.* 52 (2023) 233–241, <https://doi.org/10.1159/000528040>.
- [57] B. Lisowska-Myjak, Uremic Toxins and Their Effects on Multiple Organ Systems, *Nephron Clin. Pract.* 128 (2014) 303–311, <https://doi.org/10.1159/000369817>.
- [58] F. Husain-Syed, R. Vanholder, M.H. Rosner, H. Kawanishi, T.L. Sirich, C. Ronco, Critical Appraisal of Limitations in the Current Definition/Classification of Uremic Toxins, *Blood Purif.* 52 (2023) 221–232, <https://doi.org/10.1159/000527548>.
- [59] R. Vanholder, Introduction to the Toxins Special Issue on “Novel Issues in Uremic Toxicity”, *Toxins* 10 (2018) 388, <https://doi.org/10.3390/toxins10100388>.
- [60] W.R. Clark, N.L. Dehghani, V. Narsimhan, C. Ronco, Uremic Toxins and their Relation to Dialysis Efficacy, *Blood Purif.* 48 (2019) 299–314, <https://doi.org/10.1159/000502331>.
- [61] M. Roberts, S.W. Wong, E. Dinovo, N. Yanagawa, D.B.N. Lee, The Redy® recirculating dialysis sorbent system: Strategies to increase clearances, *ASAIO J.* 46 (2000) 212.
- [62] V. Gura, M.B. Rivara, S. Bieher, R. Munshi, N.C. Smith, L. Linke, J. Kundzins, M. Beizai, C. Ezon, L. Kessler, J. Himmelfarb, A wearable artificial kidney for patients with end-stage renal disease, *JCI Insight* 1 e86397 (2016) 86397, <https://doi.org/10.1172/jci.insight.86397>.
- [63] D.L. Ramada, J. de Vries, J. Vollenbroek, N. Noor, O. ter Beek, S.M. Mihäilä, F. Wieringa, R. Masereeuw, K. Gerritsen, D. Stamatialis, Portable, wearable and implantable artificial kidney systems: needs, opportunities and challenges, *Nat. Rev. Nephrol.* 19 (2023) 481–490, <https://doi.org/10.1038/s41581-023-00726-9>.
- [64] G. Shao, J. Himmelfarb, B.J. Hinds, Strategies for optimizing urea removal to enable portable kidney dialysis: A reappraisal, *Artif. Organs* 46 (2022) 997–1011, <https://doi.org/10.1111/aor.14185>.
- [65] Y. Ma, S. Li, M. Tonelli, L.D. Unsworth, Adsorption-based strategies for removing uremic toxins from blood, *Microporous Mesoporous Mater.* 319 (2021) 111035, <https://doi.org/10.1016/j.micromeso.2021.111035>.
- [66] F.S.C. Rodrigues, M. Faria, Adsorption- and Displacement-Based Approaches for the Removal of Protein-Bound Uremic Toxins, *Toxins* 15 (2023) 110, <https://doi.org/10.3390/toxins15020110>.
- [67] N. Florens, D. Yi, L. Juillard, C.O. Soulage, Using binding competitors of albumin to promote the removal of protein-bound uremic toxins in hemodialysis: Hope or pipe dream? *Biochimie* 144 (2018) 1–8, <https://doi.org/10.1016/j.biochi.2017.09.018>.
- [68] V. Saar-Kovrov, W. Zidek, S. Orth-Alampour, D. Fliser, V. Jankowski, E.a. L. Biessen, J. Jankowski, Reduction of protein-bound uraemic toxins in plasma of chronic renal failure patients: A systematic review, *J. Intern. Med.* 290 (2021) 499–526, <https://doi.org/10.1111/joim.13248>.
- [69] M. Faria, M.N. de Pinho, Challenges of reducing protein-bound uremic toxin levels in chronic kidney disease and end stage renal disease, *Transl. Res.* 229 (2021) 115–134, <https://doi.org/10.1016/j.trsl.2020.09.001>.
- [70] M. Roberts, The status of sorbent technology in hemodialysis treatment, *Clin. Nephrol.* 26 (Suppl 1) (1986) S44–S46.
- [71] M. Roberts, The regenerative dialysis (REDY) sorbent system, *Nephrology* 4 (1998) 275–278, <https://doi.org/10.1111/j.1440-1797.1998.tb00359.x>.
- [72] Home - Nextkidney Portable Hemodialysis Machine, Nextkidney (n.d.). <http://nextkidney.com/> (accessed September 9, 2024).
- [73] D.L. Shaffer, J.R. Werber, H. Jaramillo, S. Lin, M. Elimelech, Forward osmosis: Where are we now? *Desalination* 356 (2015) 271–284, <https://doi.org/10.1016/j.desal.2014.10.031>.
- [74] V. Sanahuja-Embuena, G. Khensir, M. Yusuf, M.F. Andersen, X.T. Nguyen, K. Trzaskus, M. Pinelo, C. Helix-Nielsen, Role of Operating Conditions in a Pilot Scale Investigation of Hollow Fiber Forward Osmosis Membrane Modules, *Membranes* 9 (2019) 66, <https://doi.org/10.3390/membranes9060066>.
- [75] P. Dou, S. Zhao, S. Xu, X.-M. Li, T. He, Feasibility of osmotic dilution for recycling spent dialysate: Process performance, scaling, and economic evaluation, *Water Res.* 168 (2020) 115157, <https://doi.org/10.1016/j.watres.2019.115157>.
- [76] E.J. Contés-de-Jesús, X. Cha, M. Flynn, The Use of Porifera Membranes for Urea Rejection in Forward Osmosis Systems, in: 44th International Conference on Environmental Systems, 2014, <https://tu-ir.tdl.org/handle/2346/59657> (accessed September 12, 2024).
- [77] C. Kim, C. Lee, S.W. Kim, C.S. Kim, I.S. Kim, Performance Evaluation and Fouling Propensity of Forward Osmosis (FO) Membrane for Reuse of Spent Dialysate, *Membranes* 10 (2020) 438, <https://doi.org/10.3390/membranes10120438>.
- [78] Acquaporin.com, Aquaporin (2023), <https://aquaporin.com/hemodialysis/ma-ke-home-dialysis-possible-aquaporin/> (accessed September 9, 2024).
- [79] E.J. Cath, S. Gormly, E.G. Beaudry, M.T. Flynn, V.D. Adams, A.E. Childress, Membrane contactor processes for wastewater reclamation in space: Part I. Direct osmotic concentration as pretreatment for reverse osmosis, *J. Membr. Sci.* 257 (2005) 85–98, <https://doi.org/10.1016/j.memsci.2004.08.039>.
- [80] D. Weerakoon, B. Bansal, L.P. Padhye, A. Rachmani, L. James Wright, G. Silyn Roberts, S. Baroutian, A critical review on current urea removal technologies from water: An approach for pollution prevention and resource recovery, *Sep. Purif. Technol.* 314 (2023) 123652, <https://doi.org/10.1016/j.seppur.2023.123652>.
- [81] G. Shao, Y. Zang, B.J. Hinds, TiO<sub>2</sub> Nanowires Based System for Urea Photodecomposition and Dialysate Regeneration, *ACS Appl. Nano Mater.* 2 (2019) 6116–6123, <https://doi.org/10.1021/acsnano.9b00709>.
- [82] J.C. Vollenbroek, A.P. Rodriguez, B.T. Mei, G. Mul, M.C. Verhaar, M. Odiijk, K.G. F. Gerritsen, Light-driven urea oxidation for a wearable artificial kidney, *Catal. Today* (2023) 114163, <https://doi.org/10.1016/j.cattod.2023.114163>.
- [83] M. Grassi, G. Kaykioglu, V. Belgiorno, G. Lofrano, Removal of Emerging Contaminants from Water and Wastewater by Adsorption Process, in: G. Lofrano (Ed.), *Emerg. Compd. Remov. Wastewater Nat. Sol. Based Treat.*, Springer, Netherlands, Dordrecht, 2012, pp. 15–37, [https://doi.org/10.1007/978-94-007-3916-1\\_2](https://doi.org/10.1007/978-94-007-3916-1_2).
- [84] A.A. Fomkin, Nanoporous materials and their adsorption properties, *Prot. Met. Phys. Chem. Surf.* 45 (2009) 121–136, <https://doi.org/10.1134/S2070205109020014>.
- [85] D. Wu, F. Xu, B. Sun, R. Fu, H. He, K. Matyjaszewski, Design and Preparation of Porous Polymers, *Chem. Rev.* 112 (2012) 3959–4015, <https://doi.org/10.1021/cr200440z>.
- [86] Z. Heidarinejad, M.H. Dehghani, M. Heidari, G. Javedan, I. Ali, M. Sillanpää, Methods for preparation and activation of activated carbon: a review, *Environ. Chem. Lett.* 18 (2020) 393–415, <https://doi.org/10.1007/s10311-019-00955-0>.
- [87] J. Lan, B. Wang, C. Bo, B. Gong, J. Ou, Progress on fabrication and application of activated carbon sphere in recent decade, *J. Ind. Eng. Chem.* 120 (2023) 47–72, <https://doi.org/10.1016/j.jiec.2022.12.045>.
- [88] T. Kameda, K. Horikoshi, S. Kumagai, Y. Saito, T. Yoshioka, Adsorption of urea, creatinine, and uric acid onto spherical activated carbon, *Sep. Purif. Technol.* 237 (2020) 116367, <https://doi.org/10.1016/j.seppur.2019.116367>.
- [89] Y.-C. Cheng, C.-C. Fu, Y.-S. Hsiao, C.-C. Chien, R.-S. Juang, Clearance of low molecular-weight uremic toxins p-creatinine, creatinine, and urea from simulated serum by adsorption, *J. Mol. Liq.* 252 (2018) 203–210, <https://doi.org/10.1016/j.molliq.2017.12.084>.
- [90] I. Geremia, R. Bansal, D. Stamatialis, In vitro assessment of mixed matrix hemodialysis membrane for achieving endotoxin-free dialysate combined with high removal of uremic toxins from human plasma, *Acta Biomater.* 90 (2019) 100–111, <https://doi.org/10.1016/j.actbio.2019.04.009>.
- [91] M.S.L. Tijink, M. Wester, J. Sun, A. Saris, L.A.M. Bolhuis-Versteeg, S. Saiful, J. A. Joles, Z. Borneman, M. Wessling, D.F. Stamatialis, A novel approach for blood purification: Mixed-matrix membranes combining diffusion and adsorption in one step, *Acta Biomater.* 8 (2012) 2279–2287, <https://doi.org/10.1016/j.actbio.2012.03.008>.
- [92] V. Wernert, O. Schäf, H. Ghobarkar, R. Denoyel, Adsorption properties of zeolites for artificial kidney applications, *Microporous Mesoporous Mater.* 83 (2005) 101–113, <https://doi.org/10.1016/j.micromeso.2005.03.018>.
- [93] K. Namekawa, M.T. Schreiber, T. Aoyagi, M. Ebara, Fabrication of zeolite-polymer composite nanofibers for removal of uremic toxins from kidney failure patients, *Biomater. Sci.* 2 (2014) 674–679, <https://doi.org/10.1039/C3BM60263J>.
- [94] L. Lu, C. Chen, C. Samarasekera, J.T.W. Yeow, Influence of zeolite shape and particle size on their capacity to adsorb uremic toxin as powders and as fillers in membranes, *J. Biomed. Mater. Res. B Appl. Biomater.* 105 (2017) 1594–1601, <https://doi.org/10.1002/jbm.b.33698>.
- [95] L. Lu, J.T.W. Yeow, An adsorption study of indoxyl sulfate by zeolites and polyethersulfone-zeolite composite membranes, *Mater. Des.* 120 (2017) 328–335, <https://doi.org/10.1016/j.matdes.2017.01.094>.
- [96] M. De Pascale, M.G. De Angelis, C. Boi, Mixed Matrix Membranes Adsorbents (MMMAS) for the Removal of Uremic Toxins from Dialysate, *Membranes* 12 (2022) 203, <https://doi.org/10.3390/membranes12020203>.





- Computational methods for adsorption study in wastewater treatment, *J. Mol. Liq.* 390 (2023) 123008, <https://doi.org/10.1016/j.molliq.2023.123008>.
- [145] C. Cazorla, The role of density functional theory methods in the prediction of nanostructured gas-adsorbent materials, *Coord. Chem. Rev.* 300 (2015) 142–163, <https://doi.org/10.1016/j.ccr.2015.05.002>.
- [146] M.P. Allen, D.J. Tildesley, Molecular dynamics, in: M.P. Allen, D.J. Tildesley (Eds.), *Comput. Simul. Liq.*, Oxford University Press, 2017, <https://doi.org/10.1093/oso/9780198803195.003.0003>.
- [147] M.P. Allen, D.J. Tildesley, Monte Carlo methods, in: M.P. Allen, D.J. Tildesley (Eds.), *Comput. Simul. Liq.*, Oxford University Press, 2017, <https://doi.org/10.1093/oso/9780198803195.003.0004>.
- [148] D. Frenkel, B. Smit, *Understanding Molecular Simulation*, 2nd ed., Academic Press Inc, USA, 2001.
- [149] C.J. Cramer, D.G. Truhlar, Density functional theory for transition metals and transition metal chemistry, *Phys. Chem. Chem. Phys.* 11 (2009) 10757–10816, <https://doi.org/10.1039/B907148B>.
- [150] F.L. de Oliveira, C. Cleeton, R.N.B. Ferreira, B. Luan, L. Sarkisov, M. Steiner, Exploring the impact of molecular force fields on the computational screening of COFs for carbon capture, in: 2023. <https://research.ibm.com/publications/exploring-the-impact-of-molecular-force-fields-on-the-computational-screening-of-cofs-for-carbon-capture> (accessed September 12, 2024).
- [151] M.P. Allen, D.J. Tildesley, Quantum simulations, in: M.P. Allen, D.J. Tildesley (Eds.), *Comput. Simul. Liq.*, Oxford University Press, 2017, <https://doi.org/10.1093/oso/9780198803195.003.0013>.
- [152] T. Yildiz, I. Erucar, Revealing the performance of bio-MOFs for adsorption-based uremic toxin separation using molecular simulations, *Chem. Eng. J.* 431 (2022) 134263, <https://doi.org/10.1016/j.cej.2021.134263>.
- [153] B. Akkoca Palabiyik, M. Batyrow, I. Erucar, Computational investigations of Bio-MOF membranes for uremic toxin separation, *Sep. Purif. Technol.* 281 (2022) 119852, <https://doi.org/10.1016/j.seppur.2021.119852>.
- [154] T. Fabiani, E. Ricci, C. Boi, S. Dimartino, M.G.D. Angelis, In silico screening of nanoporous materials for urea removal in hemodialysis applications, *Phys. Chem. Chem. Phys.* 25 (2023) 24069–24080, <https://doi.org/10.1039/D3CP01510F>.
- [155] D. Bergé-Lefranc, H. Pizzala, J.L. Paillaud, O. Schäf, C. Vagner, P. Boulet, B. Kuchta, R. Denoyel, Adsorption of small uremic toxin molecules on MFI type zeolites from aqueous solution, *Adsorption* 14 (2008) 377–387, <https://doi.org/10.1007/s10450-007-9093-6>.
- [156] V. Wernert, O. Schäf, V. Faure, P. Brunet, L. Dou, Y. Berland, P. Boulet, B. Kuchta, R. Denoyel, Adsorption of the uremic toxin p-cresol onto hemodialysis membranes and microporous adsorbent zeolite silicalite, *J. Biotechnol.* 123 (2006) 164–173, <https://doi.org/10.1016/j.jbiotec.2005.11.009>.
- [157] B. Li, S. Gong, P. Cao, W. Gao, W. Zheng, W. Sun, X. Zhang, X. Wu, Screening of Biocompatible MOFs for the Clearance of Indoxyl Sulfate Using GCMC Simulations, *Ind. Eng. Chem. Res.* 61 (2022) 6618–6627, <https://doi.org/10.1021/acs.iecr.2c00283>.
- [158] A.M. Jahromi, M. Khedri, M. Ghasemi, S. Omrani, R. Maleki, N. Rezaei, Molecular insight into COF monolayers for urea sorption in artificial kidneys, *Sci. Rep.* 11 (2021) 12085, <https://doi.org/10.1038/s41598-021-91617-1>.
- [159] T. Skorjanc, D. Shetty, F. Gándara, S. Pascal, N. Naleem, S. Abubakar, L. Ali, A. K. Mohammed, J. Raya, S. Kirmizialtin, O. Siri, A. Trabolsi, Covalent Organic Framework Based on Azacalix[4]arene for the Efficient Capture of Dialysis Waste Products, *ACS Appl. Mater. Interfaces* 14 (2022) 39293–39298, <https://doi.org/10.1021/acsmi.2c06841>.
- [160] P. Zandi, E. Ghasemy, M. Khedri, A. Rashidi, R. Maleki, A. Miri Jahromi, Shedding Light on Miniaturized Dialysis Using MXene 2D Materials, A Computational Chemistry Approach, *ACS Omega* 6 (2021) 6312–6325, <https://doi.org/10.1021/acsomega.0c06118>.
- [161] K. Karimi, M. Rahsepar, Optimization of the Urea Removal in a Wearable Dialysis Device Using Nitrogen-Doped and Phosphorus-Doped Graphene, *ACS Omega* 7 (2022) 4083–4094, <https://doi.org/10.1021/acsomega.1c05495>.
- [162] A. Miri Jahromi, P. Zandi, M. Khedri, E. Ghasemy, R. Maleki, L. Tayebi, Molecular insight into optimizing the N- and P-doped fullerenes for urea removal in wearable artificial kidneys, *J. Mater. Sci. Mater. Med.* 32 (2021) 49, <https://doi.org/10.1007/s10856-021-06525-7>.
- [163] Z. Jokar, A. Khademiyan, M.-A. Fallah, K. Smida, S.M. Sajadi, M. Inc, Molecular dynamics simulation of urea adsorption on various nanoparticles in a spiral microfluidic system, *Eng. Anal. Bound. Elem.* 145 (2022) 271–285, <https://doi.org/10.1016/j.enganabound.2022.09.029>.
- [164] P. Siahaan, N.A. Sasongko, R.A. Lusiana, V.D. Prasasty, M.A. Martoprawiro, The validation of molecular interaction among dimer chitosan with urea and creatinine using density functional theory: In application for hemodialysis membrane, *Int. J. Biol. Macromol.* 168 (2021) 339–349, <https://doi.org/10.1016/j.ijbiomac.2020.12.052>.
- [165] L. Cai, Y. Liu, H. Liang, Impact of hydrogen bonding on inclusion layer of urea to cellulose: Study of molecular dynamics simulation, *Polymer* 53 (2012) 1124–1130, <https://doi.org/10.1016/j.polymer.2012.01.008>.
- [166] P. Chen, Y. Nishiyama, J. Wohler, A. Lu, K. Mazeau, A.E. Ismail, Translational Entropy and Dispersion Energy Jointly Drive the Adsorption of Urea to Cellulose, *J. Phys. Chem. B* 121 (2017) 2244–2251, <https://doi.org/10.1021/acs.jpcc.6b11914>.
- [167] B. Widom, Some Topics in the Theory of Fluids, *J. Chem. Phys.* 39 (1963) 2808–2812, <https://doi.org/10.1063/1.1734110>.
- [168] M. Tong, Y. Lan, Q. Yang, C. Zhong, Exploring the structure-property relationships of covalent organic frameworks for noble gas separations, *Chem. Eng. Sci.* 168 (2017) 456–464, <https://doi.org/10.1016/j.ces.2017.05.004>.
- [169] A.V. Kustov, N.L. Smirnova, Standard Enthalpies and Heat Capacities of Solution of Urea and Tetramethylurea in Water, *J. Chem. Eng. Data* 55 (2010) 3055–3058, <https://doi.org/10.1021/je9010689>.